Research article

Identifying fluid-fluxed versus decompression melting in the Tonga island arc – Lau back-arc region

Christoph Beier[1✉] Simon P. Turner[2] Milena V. Schoenhofen-Romer[2,3] Philipp A. Brandl[4] Karsten M. Haase[3] Lucy McGee[2,5] Richard J. Arculus[6]

[1] Research Programme of Geology and Geophysics (GeoHel), Department of Geosciences and Geography, University of Helsinki, FIN-00014, Finland
[2] School of Natural Sciences, Macquarie University, Sydney, NSW 2109, Australia
[3] GeoZentrum Nordbayern, Friedrich-Alexander Universität Erlangen-Nürnberg, Schlossgarten 5, 91054 Erlangen, Germany
[4] GEOMAR Helmholtz Centre for Ocean Research Kiel, Wischhofstr. 1-3, 24148 Kiel, Germany
[5] Department of Earth Sciences, University of Adelaide, SA 5005, Australia
[6] Research School of Earth Sciences, The Australian National University, ACT 2601, Australia

✉ **Correspondence to:** Christoph Beier: christoph.beier@helsinki.fi

Author contributions: Conceptualization: ChB, SPT, PAB, KMH, RJA; Data curation: ChB, MVS-R, KMH, LMcG; Funding acquisition: ChB, PAB; Investigation: ChB, MVS-R, KMH, LMcG; Methodology: ChB, MVS-R, LMcG; Project administration: KMH, RJA; Visualization: ChB; Writing – original draft: ChB, SPT, MVS-R, PAB, KMH.

Data, code, and outputs: https://doi.org/10.1594/PANGAEA.978496

Submitted: 2025-03-12
Accepted: 2025-09-15
Published: 2025-11-05

Production editor:
James Darling

Handling editor:
Abigail Barker

Reviews:
David Peate,
Adam Kent

Copyediting:
Anselm Loges,
Marthe Klöcking

Partial melting at destructive plate margins is usually linked to fluid addition from the subducting plate, but decompression melting and asymmetric "wet" and "dry" wings of the melting zone at back-arc spreading centres have also been invoked. Distinguishing between these models has proved difficult using conventional geochemical data. Here, we combine $^{230}U-^{238}Th$ disequilibria, H_2O contents and Ba/Nb ratios on glasses to identify fluid-fluxed versus decompression melting across the Tonga Arc – Lau back-arc. From the arc front into the back-arc, ($^{230}U/^{238}Th$) disequilibria range from 0.55 to 1.14, H_2O contents from 2 to 0.25 wt% and Ba/Nb ratios from 1000 to 5. The ($^{230}U/^{238}Th$) disequilibria and ratios of fluid mobile to immobile trace elements are amongst the most extreme reported from arcs and change to values typical of mid-ocean ridges. Our data provide evidence for the co-existence of both fluid-fluxed and decompression melting regimes and suggest that back-arcs situated close to the arc may be able to draw subduction-related material into the spreading axis. The systematic compositional change with increasing distance between arc and back-arc does not reflect changes in dehydration reaction in the subducting slab, but different proportions of slab material contributing to the back-arc spreading regime. A stepwise change at >100 km distance between arc and back-arc marks the separation between fluid-fluxed and decompression melting domains occurring over relatively short spatial distances. These are also associated with a transitional change in ridge morphology due to the appearance of an axial magma chamber at the southern East Lau Spreading Centre.

1 Introduction

Subduction, partial melting, and crustal recycling at destructive plate margins are important geodynamic processes affecting the evolution of the Earth (e.g. Davies, 1999). As reviewed by Tatsumi and Eggins (1995), magma generation in the mantle wedge beneath arc volcanoes is usually inferred to be linked to fluid addition from the subducting plate. Decompression melting in the upwelling parts of the mantle wedge and mélange diapirs have also been invoked beneath the arc front, whereas asymmetric "wet" and "dry" areas may exist in the back-arc melting region (Bourdon et al., 1999; Conder et al., 2002; Langmuir et al., 2006; Marschall and Schumacher, 2012; Turner et al., 2004, 2006). Geochemical data have been generally successful in tracing the different components which contribute to the compositional range in the erupted lavas (Pearce and Parkinson, 1993; Pearce and Peate, 1995; Tatsumi and Eggins, 1995). The geochemical variability observed along and across island arcs has commonly been associated with changes in the residual source composition of the underlying mantle wedge combined with changes in fluids or melts originating from the metamorphic dehydration reactions in the subducting slab (Bebout, 2007; Timm et al., 2016; Tollstrup et al., 2010; Woodhead et al., 1998). These dehydration reactions are largely due to the destabilisation of pargasite and phlogopite at ~3.5 GPa and ~6.5 GPa (Spandler and Pirard, 2013), respectively.

Back-arc spreading centres that are situated angular to their adjacent island arc typically encompass a range of slab depths and provide a unique means to assess the compositional and melting changes as a function of distance to the active arc, and above the subducting slab. The enrichment from slab components may be the direct result of dehydration reactions in the subducting slab. Alternatively, they could be caused by slab rollback in which an island arc progressively moves away from the back-arc, sampling pre-depleted mantle re-enriched by slab fluids (Pearce et al., 1994), or they could be the result of melt mixing in overlapping melting zones (Zhao et al., 1997). In these cases, the variability of geochemical signatures along the back-arc do not directly reflect the dehydration reactions from the subducting slab. The interaction, or lack thereof, of the melting regions underneath the arc and back-arc remain disputed (Cooper et al., 2022; Escrig et al., 2012; Langmuir et al., 2006; Pearce et al., 2005; Taylor and Martinez, 2003).

However, identifying the mantle melting regime is challenging. Uranium-series isotope disequilibria have proved critical in this respect, being sensitive to melting rates. Additionally, U-series disequilibria in fluid-fluxed and decompression melting typically have a diametrically opposite sense (coupled ^{238}U and ^{226}Ra excesses versus ^{230}Th and ^{231}Pa excesses, respectively (Bourdon et al., 2003b)). Combined with volatile contents, U-series isotopes provide a unique means to distinguish between decompression and fluid-fluxed melting (Lundstrom, 2003; Turner et al., 2003). Few studies to date used U-series isotopes to systematically investigate the distribution and styles of melting in back-arcs with increasing distance from the arc (Beier et al., 2010; Caulfield et al., 2012; Fretzdorff et al., 2003; Peate et al., 2001).

The Valu Fa Ridge (VFR), Eastern Lau (ELSC), and Central Lau spreading centres (CLSC) in the western Pacific are situated at an increasing distance from the active Tonga island arc from south to north (Arai and Dunn, 2014; Bevis et al., 1995; Stewart et al., 2022; Taylor et al., 1996; Zellmer and Taylor, 2001) (Fig. 1). The southern VFR (SVFR) is less than 30–50 km distant from the active arc front (Sleeper and Martinez, 2014) and distances exceed 150 km at the northern termination of the CLSC (Escrig et al., 2009). Underneath the back-arc, the depth of the subducting slab increases northward from ~120–140 km underneath the VFR to >250 km at the northern end of the CLSC (Fig. 1) (Hayes et al., 2012) making this region ideally suited to determine large scale compositional and melting changes along the VFR and CLSC. Seismic data and numerical models provide complementary insights into melting processes by constraining the likely temperature profile and convection patterns in the mantle wedge at a resolution of kilometres to 10s of kilometres (Syracuse et al., 2010).

Here, we present a unique combination of geochemical and U-series data on the same samples along with published seismic data to identify the relative roles of fluid-fluxed versus decompression melting in the Tonga Arc – Lau back-arc region. We can show that the systematic changes in U-series and trace element signatures along the Lau back-arc likely are the result of direct interaction of the melting regimes, whereas a sudden change towards a dry, MORB-like melting regime occurs at a distance of >100 km between the arc and the back-arc. The occurrence of slab-related geochemical signatures along the Lau back-arc in the north and at >100 km distance between the arc and back-arc spreading centre may best be explained by reactivation (remelting and/or assimilation) of hydrous components from ancient arc components due to slab rollback. We conclude that the stepwise change in geochemical signatures at ~100 km distance between the arc and the back-arc spreading centre reflects a separation of the fluid-flux and decompression dominated melting regimes. Our model indicates that the width of the melting zone underneath the back-arc spreading centre likely extends ~50–80 km to either side of the spreading axis in line with geophysical observations from mid-ocean ridges.

2 Background and setting

The intra-oceanic Tonga island arc in the southwest Pacific and associated Lau back-arc basin (Fig. 1) has provided much important information on the geodynamics and evolution of oceanic arc-back-arc systems outlined above. The Tonga island arc was the locality where geophysical observations first identified plate subduction (Sykes, 1966). Here, as in many other oceanic arcs, geochemical tracers such as ^{10}Be and Ba/Nb have clearly identified contributions from both sediment melts and fluids, respectively, transported by the subducting Pacific plate (George et al., 2005; Turner et al., 2006). Extreme U-series isotope disequilibria in the arc front lavas have been used to determine fluid addition, melt generation and magma ascent rates and provided evidence for the effects of decompression melting subsequent to fluid flux melting (Bourdon et al., 1999; Turner et al., 2001; Turner and Hawkesworth, 1997; Turner et al., 2006). Mapping of the spatial distribution of the Pb isotope signature of the Louisville Ridge (Fig. 1a) was used to identify decoupling between the subducting plate and convection in the mantle wedge flow at depths shallower than 80 km (Beier et al., 2017b; Regelous et al., 1997; Turner and Hawkesworth, 1997). When combined with the fast convergence rates and plate age structure, this has led to the recognition that Tonga-Kermadec is the coldest subduction system on Earth (Syracuse et al., 2010) hence melting of the igneous subducting slab appears unlikely (Wei et al., 2017). More recently, across-arc seismic profiles have been used to image the location and eastward-directed influx of hot upwelling mantle in the wedge (Wei et al., 2015).

In a prior study, Caulfield et al. (2012) calculated slab surface temperatures along the Fonualei Rift and Spreading Centre (FRSC, Fig. 1) that extends from the Tonga Arc into the Lau Basin and compared these, along with geochemical data and U-series disequilibria, with experimental data for slab dehydration and sediment melting. They found evidence for both fluid-fluxed and decompression melting but the dataset was too limited to determine whether the melting regime underwent a progressive or stepwise change with increasing slab surface temperatures as well as the relative changes along the spreading axis – topics which we address here. At the time, there was also less seismic data for the temperature structure within the mantle wedge. Here, we build upon the earlier geochemical and U-series assessments by Peate et al. (2001) and Caulfield et al. (2012) by combining them with the detailed seismic profiles constructed by Wei et al. (2015) and new geochemical data from across-arc traverses to develop an integrated assessment of melting processes beneath this region.

The Lau Basin is a large V-shaped back-arc basin with numerous individual spreading centres that extends behind the Tonga island arc from ∼22.9° S to ∼15° S. The VFR, ELSC, Intermediate Lau spreading centre (ILSC) and CLSC are situated from 18° S and 22.9° S, respectively (Fig. 1) (Davy and Collot, 2000; Hawkins and Melchior, 1985; Jenner et al., 1987). The opening of the Lau Basin back-arc spreading centres has been successively propagating in a southward direction since 5.0–5.5 Ma (Fretzdorff et al., 2006; Hawkins, 1995a,b). As a result, the VFR, and Lau spreading centres are situated at an increasing distance to the arc front from as close as ∼30 km at the southern tip of the VFR at ∼22.9° S to as far as ∼110 km at 19.3° S, exceeding 150 km as one approaches the CLSC in the north (Fig. 1). The current phase of spreading started at 3–4 Ma (Escrig et al., 2009) and rates of spreading vary from almost 90 mm/a at ∼18° S to 65 mm/a at the southern tip (Taylor et al., 1996) associated with changes in rate of subduction from 160 mm/a in the north to 80 mm/a in the south (Escrig et al., 2009; Taylor et al., 1996).

The water depth decreases from N to S from 3 000–2 700 to 2 200–1 800 metres below sea level at the VFR, respectively (Escrig et al., 2009). The ELSC is split into several first-order ridge segments in which each northern segment is shifted west, relative to its southern counterpart (Escrig et al., 2009; Sleeper and Martinez, 2014). At 20.6° S, a distinct change in ridge geometry (Dunn and Martinez, 2011; Sleeper and Martinez, 2014) and geochemistry (Escrig et al., 2009) has been observed. At this latitude the ridge morphology changes from an axial depression and constant water depths north of 20.6° S to a well-defined axial high and southward decreasing depths associated with southward increasing La/Sm, Th/La, and $^{206}Pb/^{204}Pb$ ratios. These changes are coupled with a steep transition in slab depth (Hayes et al., 2012) from 160 km to > 400 km in the north (Fig. 1).

The VFR is about 160 km long and is located around 180 km west of the Tonga Trench (Fretzdorff and Haase, 2002; Massoth et al., 2007) (Fig. 1). The VFR has been active for ∼0.7–0.9 Ma (Morton and Pohl, 1990) and the spreading rate increases from 39 to 60 mm/a from S to N, along with an increase in distance to the southern Tonga Arc from 30 to 50 km (Zellmer and Taylor, 2001). The VFR consists of three overlapping, left-(westward)stepping spreading segments (Wiedicke and Collier, 1993) that are termed Northern (N-), Central (C-) and Southern (S-) VFR (von Stackelberg et al., 1990). A magma chamber underneath the ridge axis extends for at least 100 km along the axis at a depth of ∼3 km and has a width of 2–3 km (Collier and Sinha, 1990; Morton and Sleep, 1985), likely decreasing in thickness towards the north (Fretzdorff et al., 2006). Published data from the SVFR show that the erupted lavas are basaltic to rhyolitic and display typical subduction zone trace element signatures with increased fluid-mobile to -immobile element ratios (e.g. Ba/Nb, Ba/La) and relatively depleted high field strength elements (HFSEs) (Taylor and Martinez, 2003) relative to normal MORB. The southern tip of the VFR (profile E in Fretzdorff et al., 2006) was sampled during R/V Sonne cruises 67 and 167 (Fretzdorff et al., 2006; Haase et al., 2009) and sampling has been performed along, as well as across the VFR (Fig. 1b and c).

3 Samples and analytical methods

3.1 Samples

For the purpose of this contribution, we combine new data from whole rock (116) and glass (148) samples from R/V Sonne expeditions SO35 (1984), SO67 (1990), SO167 (2002) (Stoffers et al., 2003), R/V Southern Surveyor Tonga-Eastern Lau Vents (TELVE, SS02/2003, 2003) and the R/V Nadir NAUTILAU expeditions (1989) (Haase et al., 2009; The Nautilau Group, 1990). In addition, we present new combined major element, trace element, H_2O and Pb for 39 samples, and U-Th (n = 12) and Ra isotope data (n = 7), 6 of which come from a 27–47 km transect orthogonal to the arc at the southern tip of the VFR situated from 22.79° to 22.88° S and 176.88° to 176.69° W (Fig. 1c).

We integrate our new data with published data from the ELSC and VFR (Bach et al., 1998; Boespflug et al., 1990; Cooper et al., 2022; Escrig et al., 2009; Ewart et al., 1998; Falloon et al., 1992; Frenzel et al., 1990; Fretzdorff et al., 2006; Gill, 1976; Haase et al., 2009; Hawkins, 1976; Hawkins and Melchior, 1985; Hilton et al., 1993; Jenner et al., 1987; Karrei, 2008; Kent et al., 2002; Pearce et al., 1994; Peate et al., 2001; Tian et al., 2008; Vallier et al., 1991) and compare these to data from the FRSC (Caulfield et al., 2012; Keller et al., 2008) and the Tonga Arc (Cooper et al., 2022; Ewart et al., 1994, 1998; Ewart and Hawkesworth, 1987; Regelous et al., 1997; Turner and Hawkesworth, 1997).

3.2 Analytical methods

The majority of the whole rock and glass samples were processed with the sample batches discussed in Haase et al. (2002), Haase et al. (2006) and Fretzdorff et al. (2006)

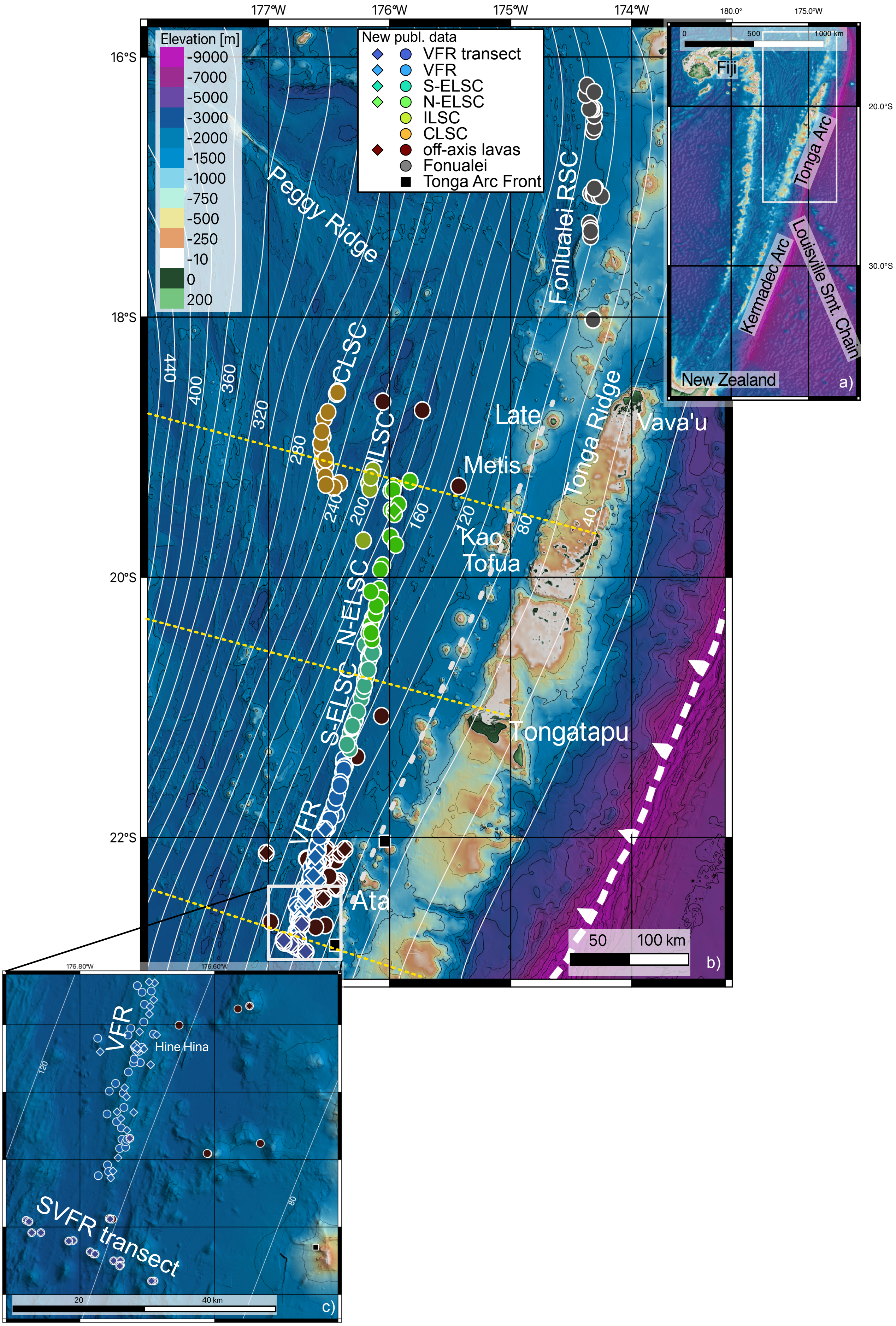
177°W
176°W
175°W
174°W
16°S
18°S
20°S
22°S
Elevation [m]
-9000
-7000
-5000
-3000
-2000
-1500
-1000
-750
-500
-250
-10
0
200
New publ. data
VFR transect
VFR
S-ELSC
N-ELSC
ILSC
CLSC
off-axis lavas
Fonualei
Tonga Arc Front
Peggy Ridge
Fonualei RSC
CLSC
ILSC
N-ELSC
S-ELSC
VFR
Late
Metis
Tonga Ridge
Vava'u
Kao
Tofua
Tongatapu
Ata
50
100 km
b)
Fiji
Tonga Arc
Kermadec Arc
Louisville Smt. Chain
New Zealand
a)
VFR
Hine Hina
SVFR transect
c)

Figure 1. *(Previous page)* a) regional overview map; b) map with sample locations showing major features and symbols used in figures and the location of seismic profiles (yellow dotted lines) from Wei et al. (2015). Fonualei Rift and Spreading Centre (Fonualei RSC) data are from Caulfield et al. (2012). Central Lau Spreading Centre (CLSC), East Lau Spreading Centre (ELSC), Intermediate Lau Spreading Centre (ILSC) and Valu Fa Ridge (VFR) are from in Escrig et al. (2009) and are also shown in Stewart et al. (2022). S-ELSC and N-ELSC as published in Escrig et al. (2009) and separated at 20.6° S. Published data are compiled from GEOROC (Bach et al., 1998; Boespflug et al., 1990; Cooper et al., 2022; Escrig et al., 2009; Ewart et al., 1998; Falloon et al., 1992; Frenzel et al., 1990; Fretzdorff et al., 2006; Gill, 1976; Haase et al., 2009; Hawkins, 1976; Hawkins and Melchior, 1985; Hilton et al., 1993; Jenner et al., 1987; Karrei, 2008; Kent et al., 2002; Pearce et al., 1994; Pearce and Peate, 1995; Peate et al., 2001; Tian et al., 2008; Vallier et al., 1991) and references therein. Slab depth (thin grey lines) from Hayes et al. (2012). Arc front is marked by thicker, dotted grey line. Inset c) shows the southern Valu Fa transect discussed in the main text.

using the same methodologies and reference materials (see Beier et al., 2025).

Major elements of glasses were analysed at the Institut für Geowissenschaften, Christian-Albrechts Universität zu Kiel using methods described in Haase et al. (2006) and Fretzdorff et al. (2006). Selected whole rock major elements were processed using methods described in Haase et al. (2002) and Fretzdorff et al. (2006). Trace element and Pb isotope analysis for whole rocks and glasses are described in Haase et al. (2006) and Fretzdorff et al. (2006). Major elements of TELVE glasses (Beier et al., 2025) were analysed using the JEOL JXA-8200 electron microprobe at the GeoZentrum Nordbayern, Erlangen. The instrument was operated with a 10 µm, defocused beam, 15 nA beam current and a 15 kV acceleration voltage calibrated against natural glass standards (Beier et al., 2018). Precision and accuracy relative to VG-A99 (NMNH 113498-1) were better than 5 % (2σ) for all major elements (Beier et al., 2017a; Brandl et al., 2012) during the analytical period. New trace element concentrations on selected samples (Beier et al., 2025) were analysed using laser ablation inductively coupled plasma mass spectrometry (LA-ICP-MS) using an Agilent 7700 quadrupole ICP-MS coupled with a Photon Machines Excite Analyte 193 nm excimer laser ablation system with HelEx sample cell at Macquarie GeoAnalytical, Macquarie University. A laser beam of 65 µm and a measurement time of 120 s (30 s background, 60 s signal, 30 s washout) was used to analyse the volcanic glasses. SRM NIST610 glass standards were analysed after every 5th sample to correct the machine drift. The SRM NIST610 standard was used for external calibration of relative element sensitivities and ^{43}Ca data for internal calibration. The accuracy is better than 10 % for all elements (except for Li and Y with < 13 %) and the reproducibility is better than 6 % for all elements using the basaltic reference material BCR-2G (n = 9). TELVE samples (TD) were analysed in the Helsinki Geoscience Laboratories (HelLabs) using a GeoLas Pro 193 nm ArF laser coupled with an Agilent 7900 ICP-MS. The samples were ablated using 10 J/cm^2, 90 µm spot sizes and a measurement time of 120 s (40 s background, 50 s signal, 30 s washout). The samples were corrected using SRM NIST610 using ^{28}Si data for internal calibration. The long-term accuracy of SRM NIST612 as unknown is deviating less than 3 % from accepted GEOREM values, with a reproducibility of < 4 % for all elements (n = 260).

The Pb isotopes were analysed with the same sample set as those described in Haase et al. (2002) using the same methods and reference materials. Uranium-series were analysed on fresh, hand-picked, unaltered volcanic glass samples, which were washed, leached and manually re-inspected twice before the addition of spikes, dissolution and column chemistry described in Beier et al. (2010) and Turner et al. (2011). The samples were analysed at Macquarie University, Sydney, Australia. The U and Th splits were analysed on a Nu Instruments® MC-ICP-MS following the method described in Dosseto et al. (2006) and McGee et al. (2011). The accuracy was better than 3.8 %, as determined by repeated analysis of the BCR-2 international rock reference materials that was processed along with the other samples throughout the analysis. Radium cuts were analysed with a ThermoFinnigan Triton® TIMS after being loaded onto degassed Re filaments with a Ta-HF-H_3PO_4 solution to activate the Ra. The $^{228}Ra/^{226}Ra$ ratios were analysed in dynamic ion counting mode. The accuracy of BCR-2 standard analysis is 0.53 % for ^{226}Ra and 1.33 % for ($^{226}Ra/^{230}Th$) (Scott et al., 2019; Sims et al., 2013). Water measurements were performed at the Research School of Earth Sciences at the Australian National University, Canberra, Australia on the SHRIMP-SI. Handpicked glass chips were embedded in In-mounts coated with Au and analysed for $^{16}O^-$ and $^{16}O^1H^-$ described by Turner et al. (2015). Internal basaltic glass standards (n = 6 each) ND61, ND70 and 24.1 were analysed between the sample measurements to ensure reproducibility (< 1.53 % for ND70 and 24.1, 8.54 % for ND61) and accuracy (< 0.79 % for all samples). Water data were calculated by the sensitivity factor given by the standard analyses and the sample measurements.

4 Results

The critical results are shown on Figures 2 to 6 and the full dataset is available in Beier et al. (2025). We present our geochemical results with respect to their geographical placing across the southernmost VFR (VFR transect), and along the VFR, S-ELSC and N-ELSC, ILSC, and CLSC as well as off-axis lavas (Fig. 1).

The VFR samples range from ∼50 to > 75 wt% SiO_2 (Fig. 2; < 55 km distance to arc) and follow a broad trend with decreasing Al_2O_3, MgO, CaO, CaO/Al_2O_3, and increasing TiO_2, Na_2O, and K_2O contents. Most major elements display a change in slope at ∼55 wt% SiO_2 im-

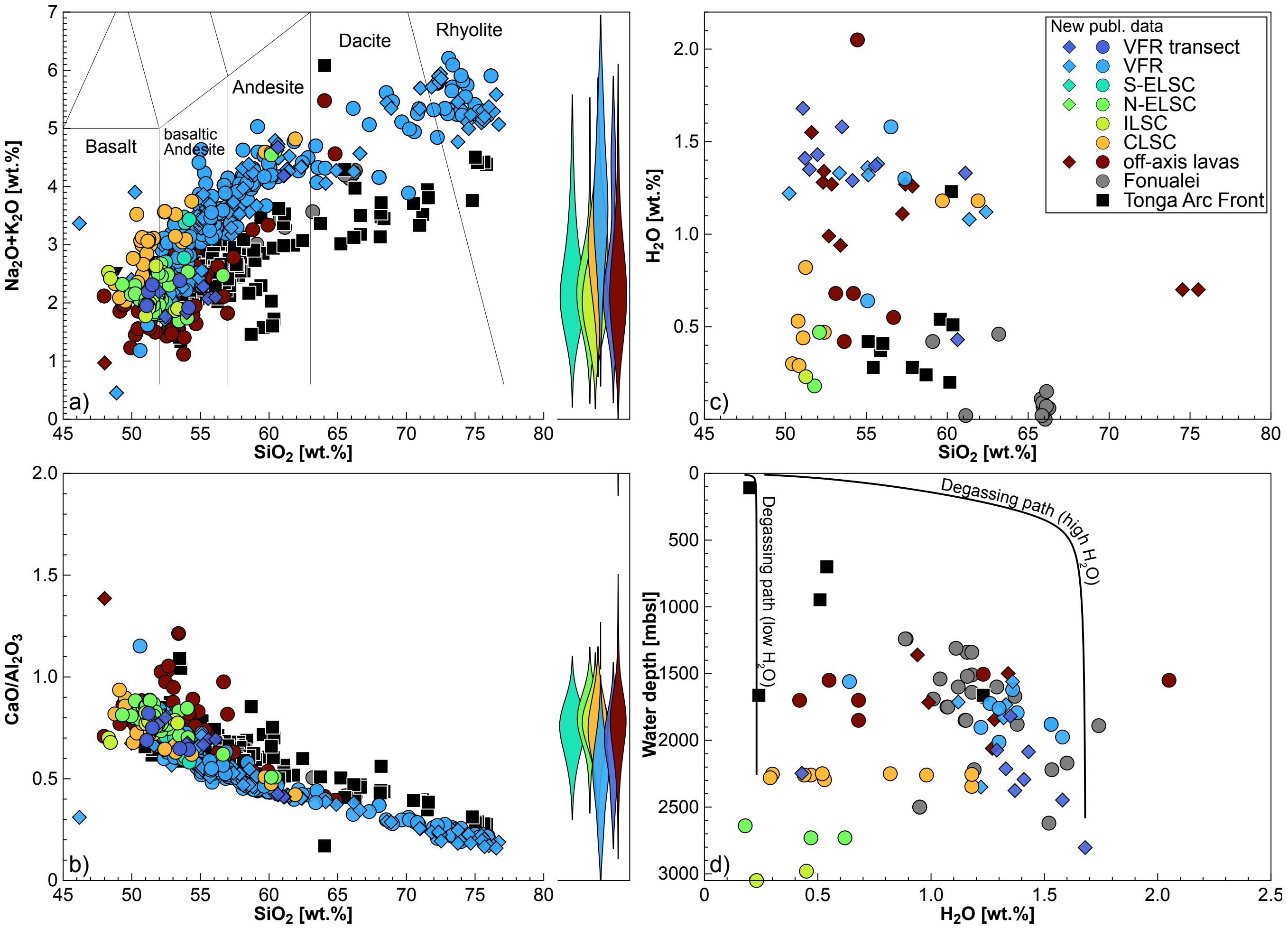

Figure 2. a) Total alkalis versus SiO_2 diagram classification after Le Maitre (1989), b) CaO/Al_2O_3 and c) H_2O versus SiO_2, and d) water depth (meters below sea level, mbsl) versus H_2O. H_2O degassing paths calculated for SO67 228KD-02 (high H_2O) and DAR0033-041-002-001 (low H_2O) (Kent et al., 2002) at ∼50 wt% SiO_2 using Sulfux_X (Ding et al., 2023) and calculated from Newman and Lowenstern (2002). Published data as in Figure 1 and Fonualei (FRSC) data are from Caulfield et al. (2012) for comparison (see main text).

plying changes in the fractionation assemblage. The VFR transect samples have a SiO_2 range of 50.9 to 59.5 wt% and are subalkaline basalts to andesites. Fractionation indices (SiO_2, MgO) display the largest variability in the VFR and southern ELSC samples. With increasing distance to the arc, samples are becoming less evolved and are mostly mafic in composition (Fig. 3a). We did not observe a clear correlation of Cl/K_2O with either MgO or SiO_2 but note that there is a positive correlation of Cl/TiO_2 with SiO_2 and that some high SiO_2 (> 65 wt%) samples are displaced towards lower Cl/TiO_2 and Cl/K_2O.

The dataset reveals several striking trends over ∼140 km from the Tonga arc front into the Lau back-arc (Fig. 3). Barium to Nb ratios (Ba/Nb), taken as a proxy for slab fluid input shows a broadly curvilinear decrease from strongly elevated ratios (> 500) to values akin to those observed in MORB (∼5.4 ± 2.1) with increasing distance from the arc front (Fig. 3b). Trace element ratios sensitive to fluid addition (e.g. Ba/Nb) are correlated with those sensitive to degree of mantle wedge depletion (e.g. Th/Yb, Nb/La, Fig. 4). Lavas from the SVFR display the highest Ba/Nb and lowest Ce/Pb ratios and cover a large range in $(Ce/Yb)_N$. Samples from the northern ELSC are closer to MORB compositions (Fig. 3 and 4) compared to the VFR. Changes in slab fluid proxies are accompanied by a broad change in glass H_2O contents that decrease from ∼2 to 0.25 wt%, but the variable H_2O contents in the arc front lavas reflect degassing and primary arc front magmas probably contain 3–5 wt% H_2O (Fig. 3d) (Cooper et al., 2022). In Pb isotope space (Fig. 5), the northern ELSC samples overlap with published data inferred for 'Indian' type MORB mantle, whereas the VFR and more southern ELSC samples have higher $^{206}Pb/^{204}Pb$ and $^{208}Pb/^{204}Pb$ ratios accompanied with elevated Ba/Nb ratios (Peate et al., 2001).

The short-lived U-Th-Ra isotope disequilibria from the VFR transect display excess of ^{238}U over ^{230}Th (Fig. 6). Our samples preserve $(^{226}Ra/^{230}Th)$ disequilibria (parentheses denote activities), implying fractionation within the last 8 ka and, therefore, no age correction is required for the Th isotope data (Fig. 6). We do not observe any correlation of $(^{230}Th/^{238}U)$ with $(^{234}U/^{238}U)$ (ranging from 0.98 to 1.01) indicating that seawater alteration has not significantly

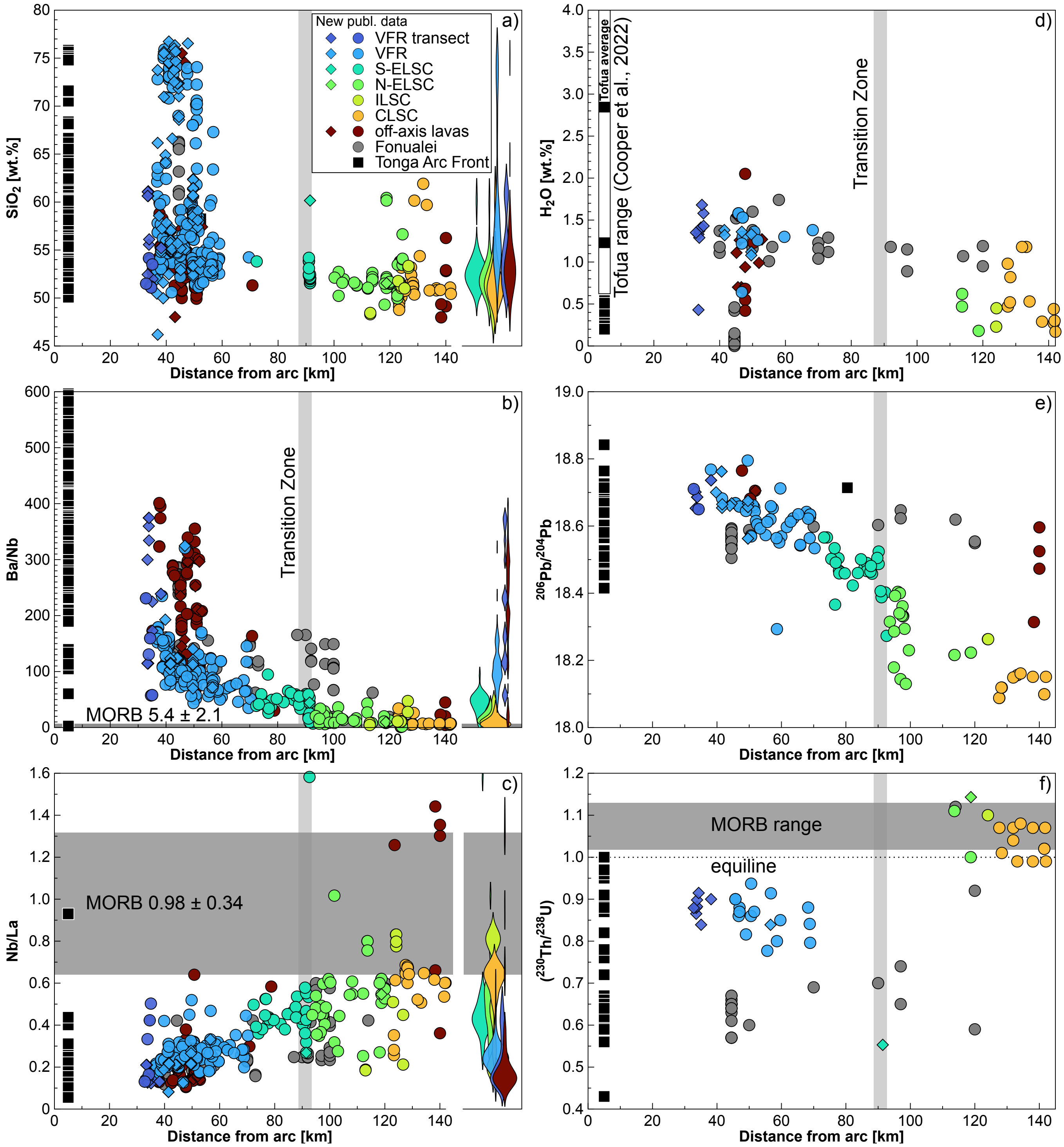

Figure 3. Plots of key geochemical parameters versus distance from arc front in km. a) SiO_2, b) Ba/Nb, c) Nb/La, d) H_2O, e) $^{206}Pb/^{204}Pb$ and f) $(^{230}Th/^{238}U)$ disequilibria (brackets denote activity ratios). Violin plots in a) to c) for clarity. Published data as in Figure 1 and 2. Tofua island data for H_2O are from Cooper et al. (2022). Grey horizontal fields mark MORB array (Jenner and O'Neill, 2012; Lundstrom, 2003), grey vertical bars mark transition zone between melting regimes as described in the main text.

affected the U-series isotope disequilibria (Chen et al., 1986) of our samples. Higher Cl/K_2O in few samples from the whole dataset could however indicate assimilation of seawater altered material (Kent et al., 2002). Uranium-Th isotope disequilibria change from large ^{238}U excesses to moderate ^{230}Th excesses at 120–140 km distance from the arc with the transition being more step-like than gradational (Fig. 3f). In the southern transect samples, slab-related fluids lead to significant ^{238}U excesses associated with elevated H_2O contents and the Ba contribution from the subducting slab (Fig. 3b and 7).

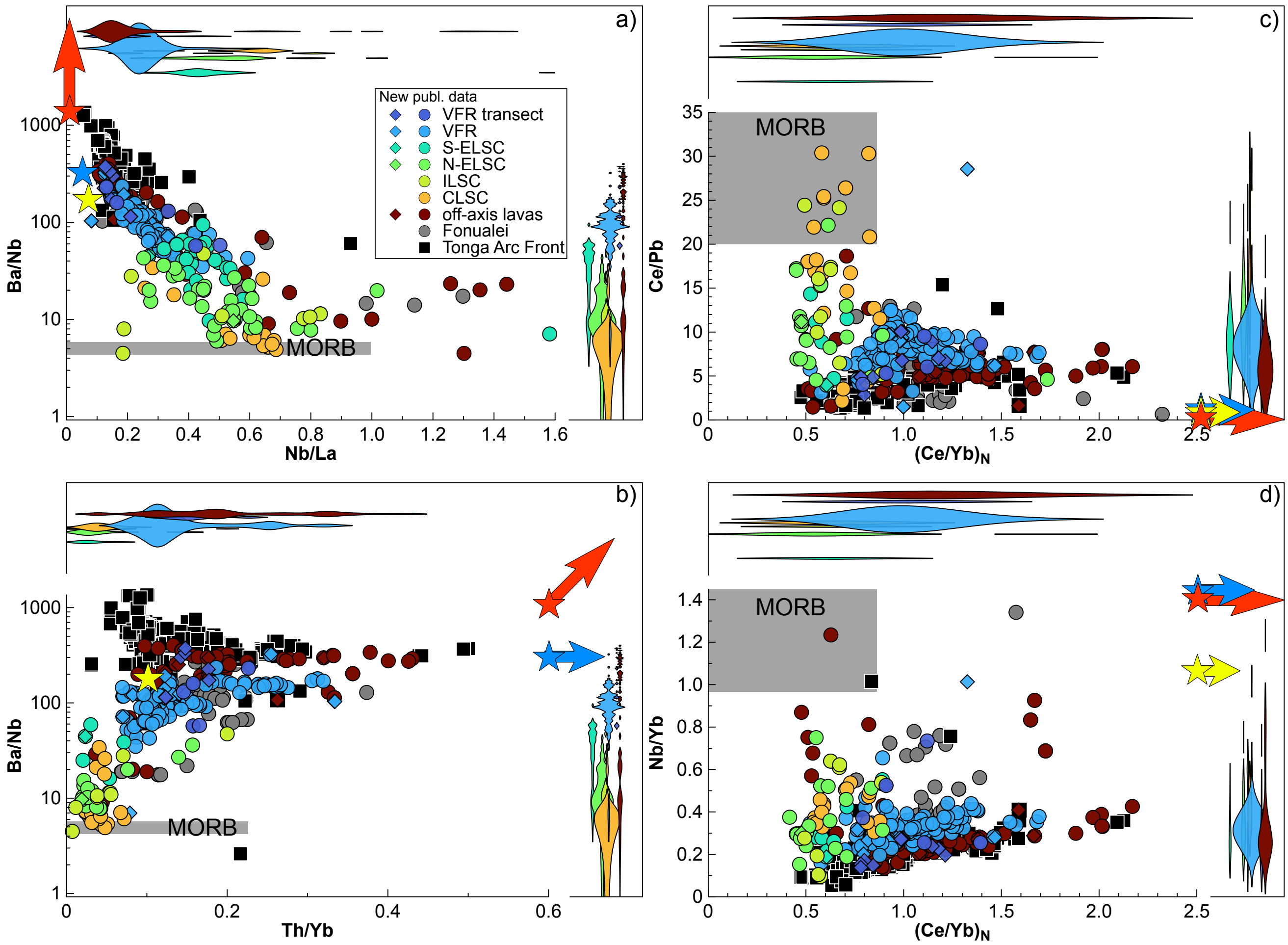

Figure 4. Plots of a) Ba/Nb versus Nb/La, b) Ba/Nb versus Th/Yb, c) Ce/Pb versus chondrite normalised $(Ce/Yb)_N$, and d) Nb/Yb versus chondrite normalised $(Ce/Yb)_N$. Chondrite values from McDonough and Sun (1995). Data sources as in Figure 1 and 2. MORB fields are compiled as averages from the database of Jenner and O'Neill (2012). Red star marks sediment fluid at 650 °C using partition coefficients from Spandler et al. (2007) and average Tonga pelagic sediment compositions from DSDP Leg 204 (Plank and Langmuir, 1993, 1998). Blue star are fluid compositions calculated from altered MORB Castillo et al. (2009) using partition coefficients by Kessel et al. (2005). Yellow star is sediment melt using sediment compositions from DSDP Leg 204 (Plank and Langmuir, 1993, 1998) at 800 °C (Johnson and Plank, 2000). Violin plots for clarity. Note that some calculated composition exceed the figure scales. Sediment fluid (red star): Ba/Nb = 7540, Th/Yb = 34, $(Ce/Yb)_N = 96$, Nb/Yb = 1.65, MORB fluid (blue star): Ba/Nb = 280, Th/Yb = 3.5, $(Ce/Yb)_N = 23$, Nb/Yb = 2.68, sediment melt (yellow star): $(Ce/Yb)_N = 3.5$, Nb/Yb = 1.1.

Samples from the SVFR have the highest H_2O contents ranging from 1.33 ± 0.14 wt% to 1.58 ± 0.03 wt% with a single outlier at 0.43 ± 0.39 wt%. A few samples are situated around the H_2O solubility curve of Newman and Lowenstern (2002) at 49 wt% SiO_2 suggesting that these samples have experienced volatile degassing, however the majority of our samples here have > 50 wt% SiO_2 suggesting that they have preserved undegassed volatile contents because SiO_2-rich compositions will be dissolving more H_2O (Fig. 2d). The SVFR samples also display the highest percentage of slab-related Ba contribution (Fig. 7a, details of the calculations in figure caption) relative to the ELSC. The VFR transect samples generally display trace element and isotope signatures that are similar to those of the neighbouring arc. The H_2O and $^{206}Pb/^{204}Pb$ contents decrease from the VFR to the northern ELSC samples associated with increasing Nb/La and $(^{230}Th/^{238}U)$, and excess ^{230}Th at 120–140 km distance to the arc front (Fig. 3 and 6). Along the ELSC the fluid-mobile to -immobile trace element ratios are negatively correlated with increasing distance to the arc front (Fig. 3), i.e. overlapping with the arc front, Ba/Nb, Th/Nb and $^{206}Pb/^{204}Pb$ decrease with increasing distance to the north. Our new H_2O data of the transect samples show increasing values with decreasing distance to the arc from the northern ELSC to the VFR (Fig. 3). At 100 km distance to the arc front, the ELSC samples approach MORB-like trace element and isotope values (Fig. 3 and 5).

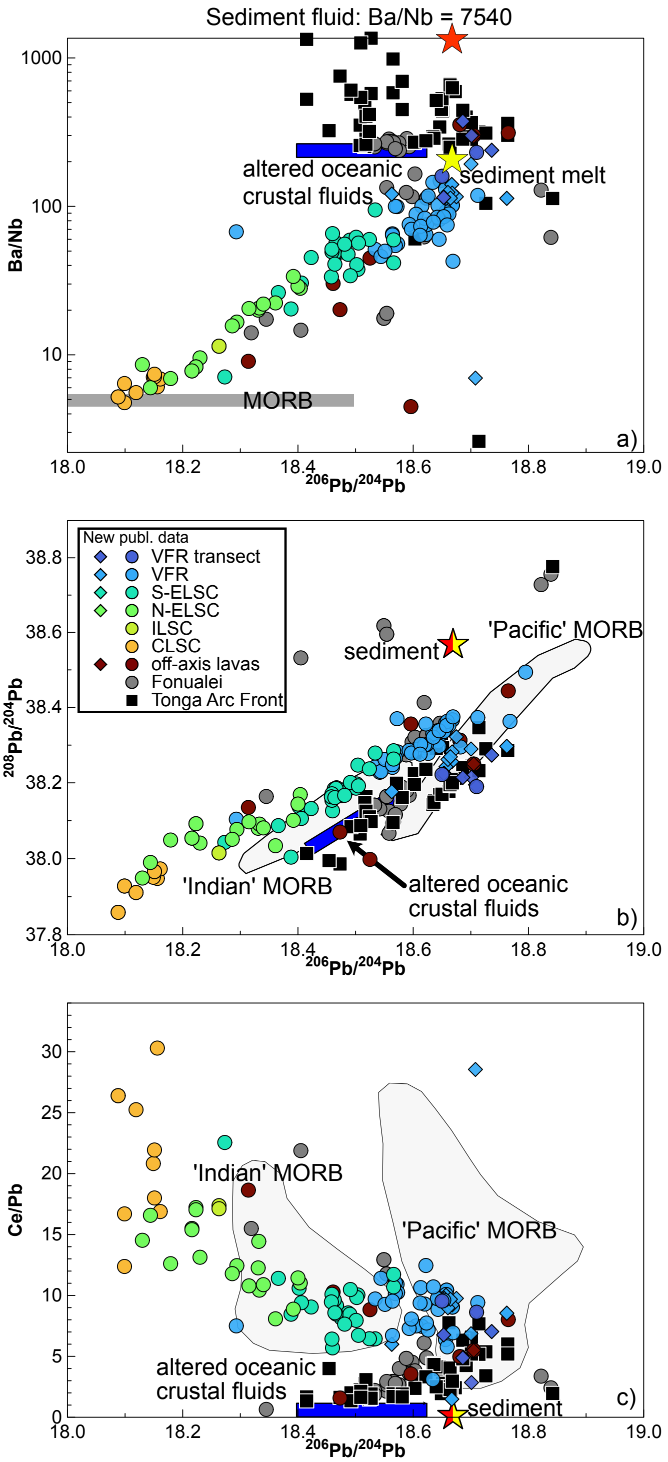

Figure 5. a) Ba/Nb, b) $^{208}Pb/^{204}Pb$ and c) Ce/Pb versus $^{206}Pb/^{204}Pb$. 'Indian' and 'Pacific' MORB from Hergt and Hawkesworth (1994) and Peate et al. (2001). Data sources as in Figures 1 and 2. Red star marks sediment fluid at 650 °C using partition coefficients from Spandler et al. (2007) and average Tonga pelagic sediment compositions from DSDP Leg 204 (Plank and Langmuir, 1993, 1998). Blue field are fluid compositions calculated from altered MORB (Castillo et al., 2009; Hergt and Woodhead, 2007; Turner and Hawkesworth, 1997) using partition coefficients by Kessel et al. (2005). Yellow star is sediment melt using sediment compositions from DSDP Leg 204 (Plank and Langmuir, 1993, 1998) at 800 °C (Johnson and Plank, 2000).

5 Discussion

For our discussion, we mainly focus on those samples for which H_2O contents and U-series disequilibria were obtained and that have < 62 wt% SiO_2 along with previously published data that have equivalent data, but we show all data in the figures (Fig. 2–7). We restrict our discussion on intermediate and mafic samples defined above to avoid extensive effects from fractional crystallisation and crustal assimilation (Heinonen et al., 2021) (Fig. 5); all samples display ^{226}Ra excess and do not require an age correction for the ($^{230}Th/^{238}U$) disequilibria (Fig. 2–7). Note that the trace element ratios used in this contribution (Fig. 2–7) are not correlated with fractionation indices (e.g. SiO_2) indicating minor influence from fractional crystallisation.

5.1 Melting and source constraints on samples recovered across the spreading axis and at the SVFR

Samples from the SVFR transect have the strongest subduction zone signatures amongst the SVFR (e.g. in Ba/Nb, Th/Nb, $^{206}Pb/^{204}Pb$, Fig. 3 and 5) overlapping with composition from the Tonga Arc (Escrig et al., 2009). The variability in incompatible and immobile elements (e.g. in Nb/La and Nb/Yb; Fig. 3 and 4) indicate the strongest degree of prior melt depletion at the SVFR (Pearce and Stern, 2006). Some of the samples with the most elevated Ba/Nb (225KD and 79DR-01) display the highest Nb concentrations of > 1 mg/kg, and elevated Nb/La and Nb/Yb (> 0.2; Fig. 4d), indicating melting of a source which is more enriched than normal MORB mantle – likely melting of sediments from the subducting slab (Fig. 4) (Pearce and Stern, 2006). In Pb isotope space, and combined with slab-fluid indicators (e.g. Ba/Nb, Fig. 5), the VFR samples exhibit a combination of both arc and back-arc characteristics with 'Indian' and 'Pacific' MORB mantle signatures, along with fluid influence derived from the subducting slab and sediment melts (Baker et al., 2004; Bézos et al., 2009; Escrig et al., 2009; Fretzdorff et al., 2006; Haase et al., 2009; Jenner et al., 1987; Peate et al., 2001). Figure 6d) shows that nearly all of the Pb, Th, U, and Ba come from the slab in the arc front and VFR magmas as fluids or melts in different mixing proportions. The 'Indian' MORB mantle likely dominates the compositional range of the mantle wedge, whereas the 'Pacific' MORB mantle compositions dominates the fluid compositions from the subducting slab; however, Peate et al. (2001) and Hergt and Woodhead (2007) note that both of these endmembers are present underneath the back-arc and also mix with an additional (sedimentary) component from the subducting slab (Fig. 4). The 'Pacific' MORB component is defined by low ($^{230}Th/^{238}U$) and $^{206}Pb/^{204}Pb$ (Fig. 6b) (Elliott, 2004; Turner and Hawkesworth, 1997), whereas VFR samples close to the equiline and with high $^{206}Pb/^{204}Pb$, Th/Yb, and $(Ce/Yb)_N$ may be a sediment melt (Fig. 4 and 6) where $D_{Th} = D_U$ (Johnson and Plank, 2000) and thus little fractionation of U and Th will occur during sediment melting (Fig. 4 and 5). Pearce and Stern (2006) define a deep, high-temperature sediment melt and a relatively shallower low temperature fluid (Fig. 5 and 6). The fluids will be

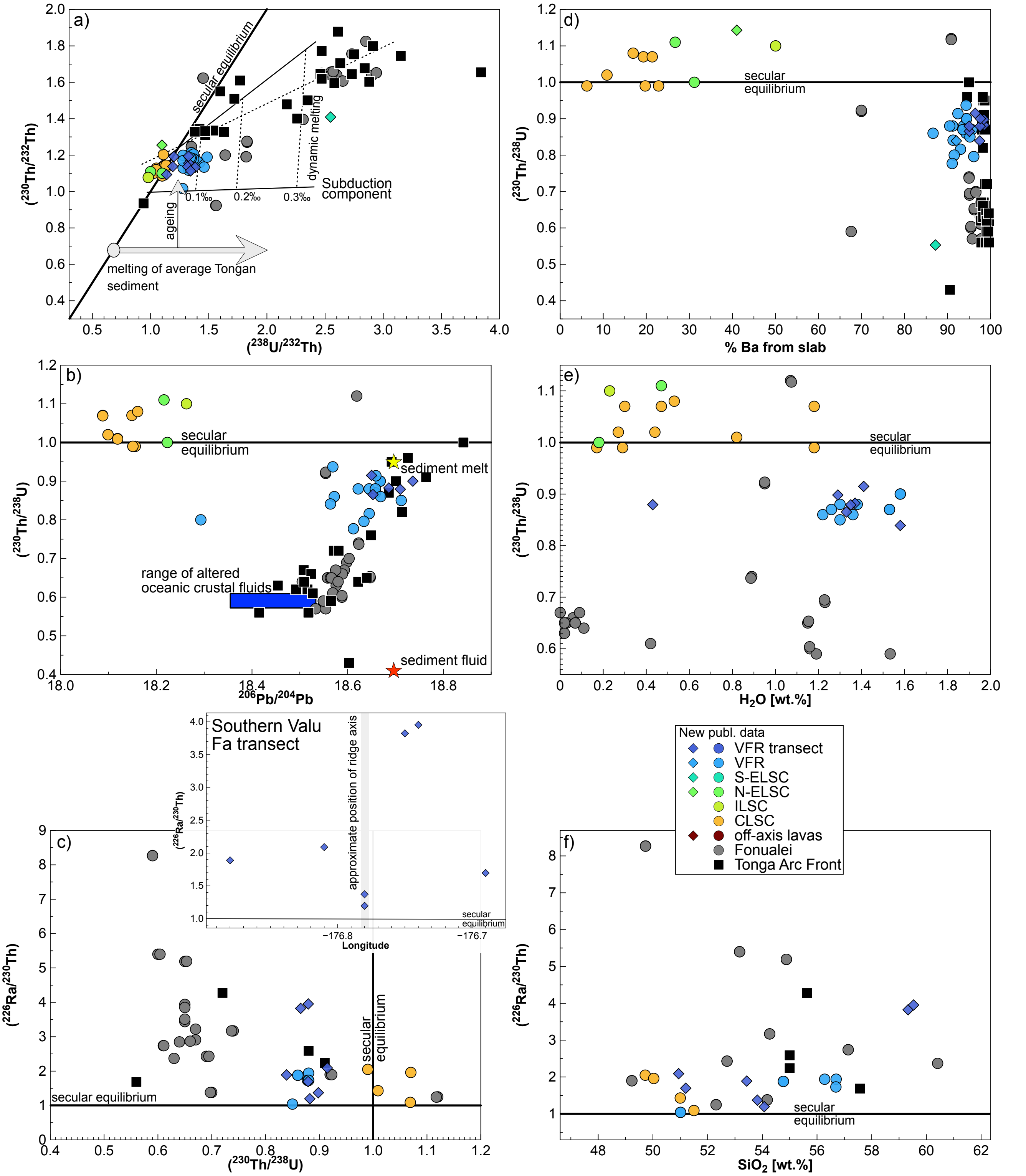

Figure 6. Plots of radiogenic isotopes and U-series disequilibria for all data. a) Equiline diagram of (^{230}Th/^{232}Th) versus (^{238}U/^{232}Th), b) (^{230}Th/^{238}U) versus ^{206}Pb/^{204}Pb, c) (^{226}Ra/^{230}Th) versus (^{230}Th/^{238}U), inset in c) shows longitudal distribution of SVFR transect samples (Fig. 1), d) (^{230}Th/^{238}U) versus % Ba contribution from the subducting slab (see Fig. 7 for details on calculations), e) (^{230}Th/^{238}U) versus H_2O, and f) (^{226}Ra/^{230}Th) versus SiO_2. Melting model in a) adapted from Beier et al. (2010), George et al. (2003), Turner et al. (2003), and Caulfield et al. (2012). Note that simplified model of the subduction component is the total contribution of a mixture of altered oceanic crust and sediment (Beier et al., 2010). Blue field are fluid compositions calculated from altered MORB (Castillo et al., 2009; Hergt and Woodhead, 2007; Turner and Hawkesworth, 1997) using partition coefficients by Kessel et al. (2005). Yellow star is sediment melt using sediment compositions from DSDP Leg 204 (Plank and Langmuir, 1993, 1998) at 800 °C (Johnson and Plank, 2000). Excess of altered oceanic crustal fluids estimated after Caulfield et al. (2012), sediment fluid excess after Kessel et al. (2005) and Bourdon et al. (2003a). Data sources as in Figures 1 and 2 (note that only samples with combined U-Th-Ra analyses are plotted in c and e).

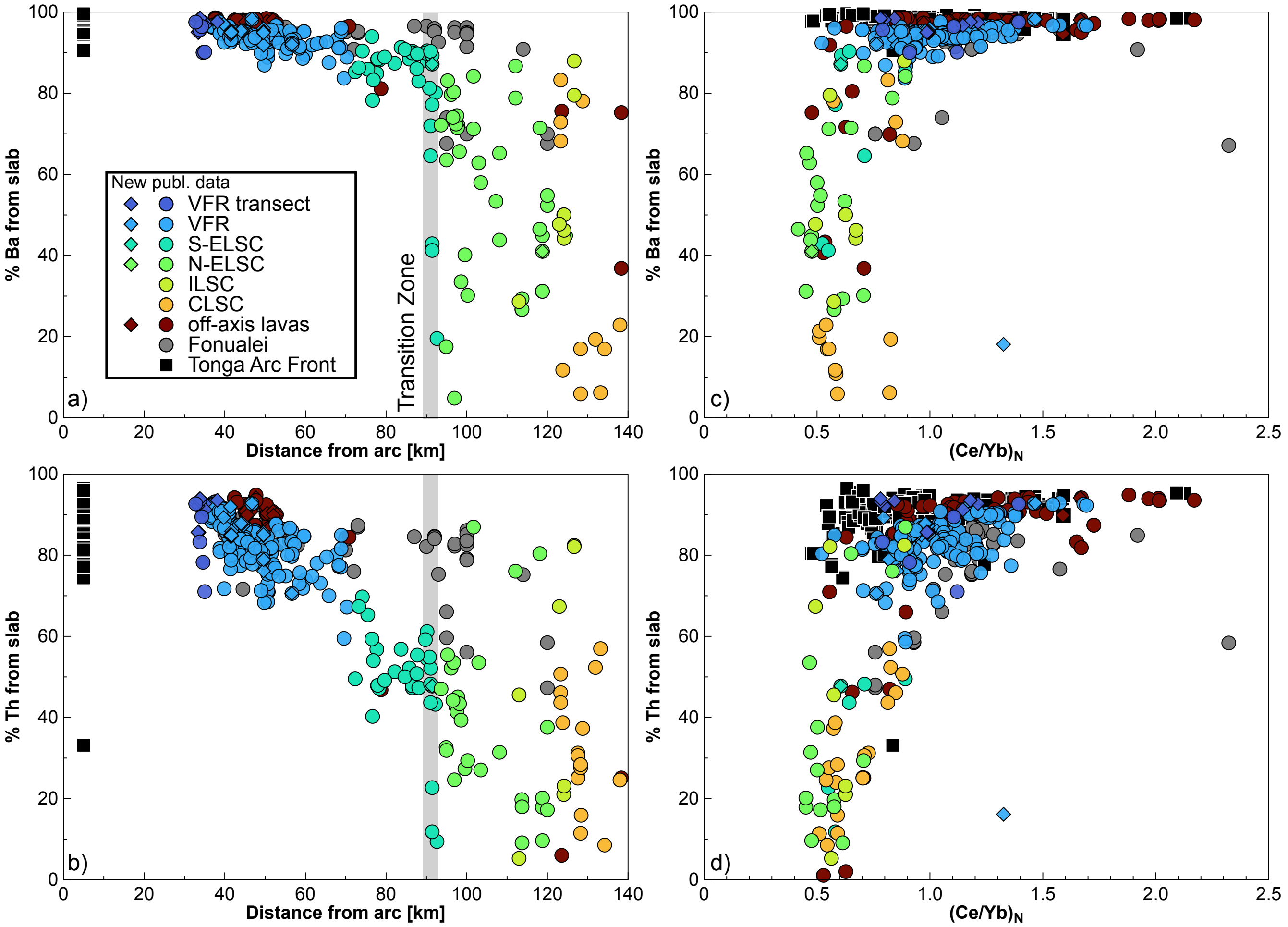

Figure 7. a) % Ba contribution from the slab and b) % Th contribution from the slab versus distance from the arc front in km; c) % Ba contribution from the slab, d) % Th contribution from the slab versus chondrite normalised $(Ce/Yb)_N$. Barium contribution from the slab was calculated using a MORB Ba/Nb of 5.71 (Jenner and O'Neill, 2012), and Th contribution was calculated using Th/Nb ratio of 0.0653 (Jenner and O'Neill, 2012). Data sources as in Figures 1 and 2. Chondrite values from McDonough and Sun (1995).

defined by relatively higher Ba/Nb and Th/Yb, and even lower Ce/Pb relative to the high temperature sediment melts (Fig. 4 and 5). The SVFR samples are geochemically comparable to ODP site 839 basalts in the Lau Basin which have been interpreted to reflect < 0.5 % sediment contribution and degrees of partial melting up to 25 % (Fretzdorff et al., 2006).

Assuming the highest H_2O contents to be ∼1.5 wt% along the VFR from our samples (Fig. 3), the primary melt composition $C^0_{H_2O}$ would be ∼0.17 wt% (Kimura and Ariskin, 2014; Portnyagin et al., 2007) comparable to Mariana Trough data (Kelley et al., 2010). The resulting melt fraction (F) would be 10–15 % combined with excess mantle wedge temperatures of less than 40 °C (Kelley et al., 2010). Modelling on-axis sample SO167 74DR-1 from the VFR (using Arc Basalt Simulator Version 5 of Kimura, 2017) indicates a 3–5 % depletion of the mantle wedge from prior melting reducing mantle fertility, e.g. due to slab rollback (Pearce and Stern, 2006). In addition, ∼3 % of the shallow and deep slab components are added to the mantle wedge and result in a melt fraction of 10–14 %.

The fluid-mobile nature of U under oxidising conditions leads to excesses of ^{238}U over ^{230}Th along arcs (Turner and Hawkesworth, 1997). In addition, the shorter-lived daughter isotope of ^{230}Th, ^{226}Ra is similarly fluid-mobile to Ba (Elliott, 2004; Turner et al., 2003) allowing Ra disequilibria to track the addition of fluids to the mantle wedge on timescales < 8 ka (Turner et al., 2001). The preservation of (^{230}Th/^{238}U) and (^{226}Ra/^{230}Th) disequilibria (Jull et al., 2002) suggests a low porosity as also supported by seismic evidence in the region (Forsyth et al., 1998). Fluid-fluxed melts have commonly been associated with larger ^{238}U excesses ((^{230}Th/^{238}U) ≪ 0.9) and elevated (^{226}Ra/^{230}Th) > 4 in zero-age arc lavas (Turner et al., 2003). Contrastingly, decompression melting of relatively dry MORB mantle causes (^{230}Th/^{238}U) disequilibria from > 0.9 to > 1. However, Beier et al. (2010) have shown that dynamic decompression melting of subduction modified, oxidised mantle may lead to ^{238}U excesses but leaves the (^{226}Ra/^{230}Th) disequilibria unaffected. The dynamic models of U-series disequilibria suggest that the southernmost spreading axis sample can be reproduced by dynamic melting of a mantle source containing a small quantity of slab-related components (Fig. 6) in line with estimates from the H_2O contents and trace element constraints (Fig. 4, 5, and 6). Thus, the presence of ^{238}U and ^{230}Th disequilibria does not require cold, buoyant diapirs or reactive transport (Hall and Kincaid, 2001; Wu et al., 2020; Zhang et al., 2020).

The two samples with ($^{226}Ra/^{230}Th$) close to equilibrium preserve excess in ^{238}U ($^{230}Th/^{238}U$) < 0.85 together with elevated fluid-sensitive ratios (e.g. Ba/Nb; Fig. 3), whereas samples with ($^{230}Th/^{238}U$) ≥ 0.9 have significant ^{226}Ra disequilibria > 1.5 indicating that these samples have less pronounced ($^{230}Th/^{238}U$) disequilibria but have been subject to melting within the last 8 ka (Fig. 6). The largest excess in ^{226}Ra is observed closest to the ridge axis suggesting that these samples are the youngest or had a larger relative fluid input. The samples with the highest ^{226}Ra also have the highest SiO_2 contents (59.6 wt%, Fig. 6), indicating that, in addition to melting, fractionation occurs on timescales of < 8 ka. At slab depths of 120–150 km along the SVFR (Hayes et al., 2012), this implies minimal rates of ascent of 15–20 m/a from the subducting slab to eruption which is at least 150–200 times the rate of spreading in the region 65–99 mm/a (Taylor et al., 1996). In contrast the signatures along the northern ELSC reflect simple decompression melts resulting in slight Th excesses (Fig. 6a).

In the vicinity of the SVFR and the nearby arc, we observe the preservation of both trace element enriched and depleted signatures with varying contributions from the subducting slab (Fig. 3), i.e. at < 55 km distance between the arc and back-arc, suggesting limited mixing and homogenisation, although seismic observations indicate a continuous magma chamber reflector underneath the morphologically segmented ridge (Sleeper et al., 2016; Wiedicke and Collier, 1993). In addition, the off-axis compositions (Fig. 3) in the vicinity of the VFR preserve a larger heterogeneity of trace element compositions suggesting that these may bypass homogenisation in an axial magma chamber similar to observations from mid-ocean ridges (Batiza, 1989; Batiza and Niu, 1992; Brandl et al., 2012). The arc lavas in the vicinity of the VFR may best be explained by mixing of depleted mantle with a shallow low-temperature sedimentary fluid and a sedimentary melt, whereas the back-arc lavas predominantly reflect mixing of a sediment melt with a depleted mantle component.

5.2 Changes in melting and source composition along the back-arc spreading axis

The distance and the nature of the transition between volatile-rich, fluid-fluxed (Langmuir et al., 2006) and decompression melting (Conder et al., 2002) in back-arcs remains not well resolved. A gradual versus stepwise transition from normal MORB to back-arc basin basalts (BABB), depends on the angle of the subducting slab and the distribution of hydrous components in the upper mantle (Beier et al., 2010), and may affect the ridge morphology (Sleeper et al., 2016). In the northern Lau Basin (Fig. 1), a systematic decrease of slab-related signatures with increasing depth of the Benioff Zone is the result of progression from a slab-related, fluid-fluxed melting regime to decompression melting (Caulfield et al., 2012). Here, we discuss the geochemical signatures along the VFR and ELSC, i.e. from south to north with increasing distance to the arc front, and a northward increasing depth to slab (Hayes et al., 2012).

Indicators of slab contribution might be anticipated to systematically vary with distance from the arc – as observed for the ELSC lavas, but our southernmost transect samples do not show such correlation. Generally, we observe the highest H_2O contents (∼ 1.5 wt%) closest to the arc and at Benioff Zone depths < 125 km (Hayes et al., 2012) at which the slab surface temperature will be < 800°C (van Keken et al., 2011). The release of H_2O from the subducting slab underneath the Tonga Arc has been estimated to peak at 100–150 km depth (van Keken et al., 2011) in agreement with our H_2O data. Samples further away (> 150 km) from the arc generally display lower H_2O contents (Loock et al., 1990; Peate et al., 2001).

Considering that Nb is relatively immobile compared to Ba and Th in the VFR and ELSC lavas, we calculate the amount of Th and Ba derived from the subducting slab using the Ba/Nb of MORB as reference. Our calculations in Figure 7 show that the northern ELSC lavas at 120–140 km distance have experienced a subtle contribution from the subducting slab ranging from ∼ 10 % to a maximum of 40–60 % for Ba and Th while lavas closer to the arc (< 65 km) consistently reflect > 80 % contribution from the subducting slab component.

We do not observe a correlation between slab-related signatures and those sensitive to degrees of partial melting (e.g. Na_8 or $(Ce/Yb)_N$ with Ce/Pb) along the ELSC, i.e. in lavas with increasing distance to the arc. Lavas erupted at 90–100 km to the arc front display a relatively large geochemical heterogeneity in Pb isotopes (Fig. 3 and 5) but relatively little variability in ratios sensitive to prior melt extraction (e.g. Nb/La, Fig. 3). The change in composition from slab-related fluids to predominantly decompression MORB melting occurs in a regional ridge transition zone (ELSC3 and ELSC4 previously also described by Escrig et al. (2009) and Jacobs et al. (2007) also associated with increasing slab depth (Fig. 1) (Hayes et al., 2012)). The compositional variability in subduction-related indices suggests a stepwise change, where the sources north of 20.6° S experience a smaller slab contribution (Fig. 3 and 8), and are increasingly dominated by relatively dry, depleted MORB sources. The occurrence of relatively high H_2O contents and samples with elevated Ba/Nb relative to MORB and an increased Ba (20–80 %) and Th (20–60 %) contribution from the slab at 100 km (Fig. 3 and 7) suggests that these magmas have experienced some form of slab contribution likely as a result of mixing along the ELSC in which these magmas are situated on mixing arrays between a relatively dry, MORB-like component and the arc-related hydrous endmember (Fig. 4). Samples from the northern ELSC display small ^{230}Th excesses (Fig. 6) (Peate et al., 2001) consistent with decompression melting (Lundstrom, 2003). Low H_2O contents and Ba/Nb ratios, less radiogenic Pb isotope ratios, and a relatively small Ba contribution

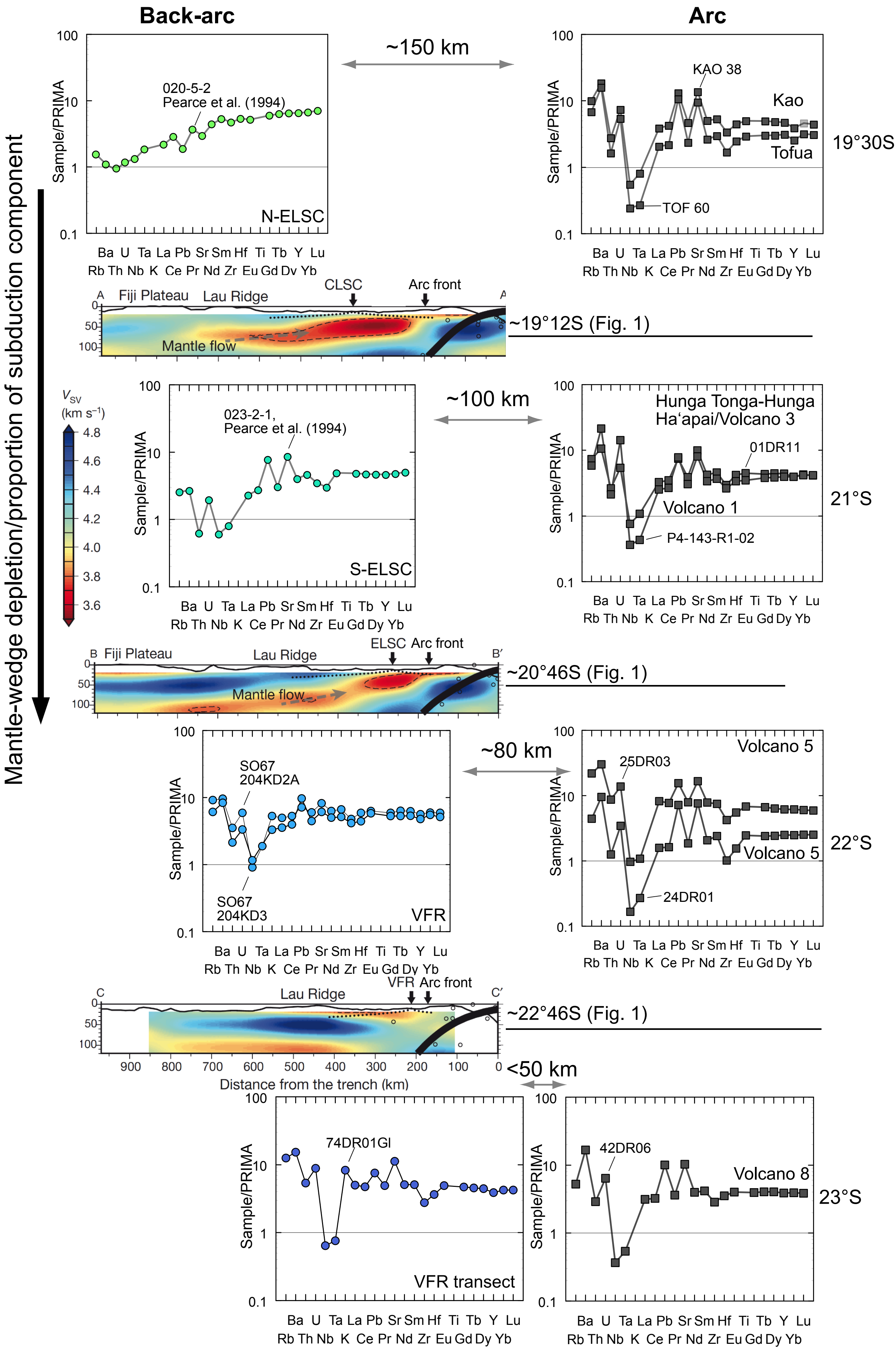

Back-arc
Arc
~150 km
020-5-2
Pearce et al. (1994)
N-ELSC
KAO 38
Kao
Tofua
TOF 60
19°30S
Sample/PRIMA
Ba U Ta La Pb Sr Sm Hf Ti Tb Y Lu
Rb Th Nb K Ce Pr Nd Zr Eu Gd Dy Yb
Fiji Plateau
Lau Ridge
CLSC
Arc front
Mantle flow
~19°12S (Fig. 1)
~100 km
023-2-1,
Pearce et al. (1994)
S-ELSC
Hunga Tonga-Hunga
Ha'apai/Volcano 3
01DR11
Volcano 1
P4-143-R1-02
21°S
Mantle-wedge depletion/proportion of subduction component
ELSC
~20°46S (Fig. 1)
~80 km
SO67
204KD2A
SO67
204KD3
VFR
Volcano 5
25DR03
24DR01
22°S
VFR
~22°46S (Fig. 1)
Distance from the trench (km)
<50 km
74DR01GI
VFR transect
42DR06
Volcano 8
23°S

Figure 8. *(Previous page)* Seismic profiles from Wei et al. (2015) combined with mantle-normalised, incompatible trace elements plots for associated samples at the arc front and back-arc with distance from arc front in km indicated. Back-arc data for N-ELSC and S-ELSC are from Pearce et al. (1994).

from the subduction slab in the northern ELSC samples (Fig. 4, 5 and 7) imply that the slab contribution may be small in this area.

Thus, magmas along the entire length of the ELSC suggest that the contribution from the subducting slab experiences a major decrease at 20.6° S (90–100 km distance from the arc; Fig. 8). At this distance the depth of the subducting slab would be > 180 km (Fig. 1) which could indicate a change towards a downward-directed flow (Cagnioncle et al., 2007). Using mantle source compositions and partition coefficients used by Beier et al. (2017b) for the northern Tongan arc volcanoes, the SVFR lavas can be modelled by melting of a mantle that has experience ∼5 % depletion in the spinel stability field prior to melting underneath the VFR. The source of the northern ELSC magmas is estimated to form from ∼20–30 % of partial melting of a source similar to that of normal MORB (Workman and Hart, 2005). This is consistent with the changes in the Pb isotope compositions and Ba/Nb that are close to MORB for both Pb isotopes and Ba/Nb (Fig. 5) (Jenner and O'Neill, 2012). The occurrence of diminished slab-related signatures several 100 km from the active arc could be explained by melting of remnant subduction components during slab roll-back (Pearce et al., 1994). Alternatively, these could be contributions from ancient, rifted arc crust as indicated by the transition in density clusters in the northern ELSC (Galley et al., 2024).

5.3 From the arc front to the back-arc: geodynamic implications from geochemistry

The change from slab-related fluid-fluxed to predominantly dry decompression melting occurs in a regional ridge transition zone (Escrig et al., 2009; Sleeper et al., 2016) where slab depth increases from 160 to 240 km (Fig. 1) (Hayes et al., 2012) and the morphology of the back-arc spreading centre changes from a deep, flat, faulted axis at ∼100 km distance from the arc to a volcanic ridge further south (Sleeper et al., 2016). This change in morphology has also been associated with the appearance of an axial magma chamber along the southern ELSC (Escrig et al., 2009; Jacobs et al., 2007). At this slab depth, fluid migration paths may also change to downward flow (Cagnioncle et al., 2007). Our new data suggest that, in the case of the SVFR, the "dry" ('MOR-like') and the "wet" ('subduction related') wings (Langmuir et al., 2006) of the melting regime may not be easily distinguishable because they are physically not clearly separated. The similarity of geochemical slab signatures across the VFR suggests that the mantle is heterogeneous on the scale of ∼10–50 km in this region involving normal and depleted MORB mantle and various subducting slab components. We propose that much of the melting regime is influenced by the relatively slow rates of spreading of 65–99 mm/a, focusing melts into the ridge axis (Sleeper et al., 2016; Taylor et al., 1996). This leads to overlapping melting zones between the arc and back-arc (Fig. 8) (Wei et al., 2015), in which melts from the subducting slab are mixed with variably depleted mantle (Sleeper and Martinez, 2014; Zha et al., 2014; Zhao et al., 1997), suggesting that back-arcs situated close to the arc draw subduction-related mantle material into the spreading axis (Schmid et al., 2020). Alternatively, partial melts from flux melting are focussed into the back-arc spreading axis. Geophysical data imply that the separation of the two melting regimes occurs at a distance of 80–100 km (Fig. 8) (Wei et al., 2015) – a distance at which the contribution of the slab components becomes small and results from along-axis mixing of melts or melting of ancient subduction components. In addition, this is the distance at which the depth of the subducting slab exceeds 150 km (Fig. 1) (Hayes et al., 2012) and in which the contribution from the subducting slab may be comparatively low due to downward flow of the slab components. The relatively sudden separation of the melting regimes and the associated change in morphology may be the result of changes in rheological properties due to a smaller contribution from the subduction slab (Cagnioncle et al., 2007; Hirth and Kohlstedt, 1996; Sleeper et al., 2016).

We conclude that, at distances of less than 100 km between the arc and associated back-arc, the widths of the melting regions are wide enough to be overlapping, producing geochemical trends that are not representative for the breakdown of minerals in the subducting slab (Fig. 8). The separation of the melting regions at distances of > 100 km between the arc and the back-arc implies that the width of the melting zone underneath the back-arc may be 50–80 km at these rates of spreading. This is less than those observed along fast-spreading mid-ocean ridges where the melting domain may exceed > 100 km on either side of the ridge (The MELT Seismic Team, 1998). We interpret this to be the result of distinct differences in the mantle flow field in the subduction zone environment (Goldberg and Holt, 2024) as opposed to a diverging flow field underneath mid-ocean ridges (Ligi et al., 2008).

6 Conclusion

We do not observe a gradual change in geochemical compositions at distances < 100 km between the arc and back-arc. This suggests that the decompression and fluid-fluxed melting regimes overlap. The geochemical heterogeneity may reflect melting of a small-scale heterogenous mantle in a fluid-flux melting regime. We also show that in the SVFR, timescales of dehydration, melting, fractionation, and eruption are likely < 8 ka. A stepwise change at distances of > 100 km between the arc and back-arc, the occurrence of excess ^{230}Th and prevalent MORB signatures suggests that melting is due to decompression and that the systematic decrease in subduction influence observed with increasing distance is likely the result of melting of hydrous remnants during slab rollback. We conclude that at spreading rates of < 100 mm/a, the width of the melting zone underneath the spreading axis is 50–80 km to each side. Our model suggests that back-arcs situated close to the arc may draw subduction-related mantle material into the spreading axis. One key observation is that the compositional change with increasing distance between the arc and back-arc does not reflect changes in dehydration reaction in the subducting slab, but rather different proportions of slab material dragged into the back-arc spreading regime. The stepwise change at > 100 km distance suggests that the separation between the fluid-fluxed arc and decompression back-arc melting domains occurs over relatively short spatial distances and may be associated with a transitional change in ridge morphology and slab related change of fluid migration.

Acknowledgements

We acknowledge chief scientists, captains, and crews of R/V Sonne and R/V Southern Surveyor for their invaluable help and remarkable efforts during numerous research expeditions and thank the entire scientific parties for their immense efforts in obtaining the samples. We particularly thank Peter Stoffers for his long-standing efforts in sampling the Tonga-Kermadec island arc and Jim Gill for truly inspiring, fruitful discussions which started in a San Francisco restaurant on a napkin. We thank Tim Worthington for help during analysis and Trevor Ireland for support during the H_2O analysis. We acknowledge two anonymous reviewers and Takeshi Kuritani who have provided helpful and constructive comments on a previous version of the manuscript. We acknowledge the constructive and helpful comments by editor Abigail Barker and reviewers Adam Kent and David Peate. We acknowledge support by the Smithsonian Institution in providing calibration and reference materials for the microprobe analyses. We acknowledge funding of the Deutsche Forschungsgemeinschaft BE4459/8-1 and BR5297/2-1 and a student fee waiver of Macquarie University in the framework of a cotutelle agreement between Macquarie University and the Friedrich-Alexander Universität Erlangen-Nürnberg. ChB acknowledges R. Sport WH and a möcki-stay in southern Finland with P. Brandl. F. Genske and E. Ranta for mental support during the final stages of this manuscript. This is HelLabs contribution #0036.

Data, code, and outputs availability

The data that support the findings of this study and the sample localities are available from Beier et al. (2025, https://doi.org/10.1594/PANGAEA.978496). Figures are available for download in the online version of this article.

Competing interests

The authors declare no competing interests.

Licence agreement

References

Arai R, Dunn RA (2014). Seismological study of Lau back arc crust: Mantle water, magmatic differentiation, and a compositionally zoned basin. *Earth and Planetary Science Letters* 390: 304–317. doi:10.1016/j.epsl.2014.01.014.

Bach W, Hegner E, Erzinger J (1998). Chemical fluxes in the Tonga subduction zone; evidence from the southern Lau Basin. *Geophysical Research Letters* 25(9): 1467–1470. doi:10.1029/98gl00840.

Baker J, Peate D, Waight T, Meyzen C (2004). Pb isotopic analysis of standards and samples using a ^{207}Pb–^{204}Pb double spike and thallium to correct for mass bias with a double-focusing MC-ICP-MS. *Chemical Geology* 211(3): 275–303. doi:10.1016/j.chemgeo.2004.06.030.

Batiza R (1989). Seamounts and seamount chains of the eastern Pacific. In Winterer E, Hussong D, Decker R (eds.) *The eastern Pacific Ocean and Hawaii*, vol. N of *The geology of North America*. Geological Society of America. doi:10.1130/DNAG-GNA-N.

Batiza R, Niu Y (1992). Petrology and magma chamber processes at the East Pacific Rise approximately 9°30'N. *Journal of Geophysical Research, B, Solid Earth and Planets* 97(5): 6779–6797. doi:10.1029/92JB00172.

Bebout GE (2007). Metamorphic chemical geodynamics of subduction zones. *Earth and Planetary Science Letters* 260(3-4): 373–393. doi:10.1016/j.epsl.2007.05.050.

Beier C, Brandl PA, Lima SM, Haase KM (2018). Tectonic control on the genesis of magmas in the New Hebrides arc (Vanuatu). *Lithos* 312-313: 290–307. doi:10.1016/j.lithos.2018.05.011.

Beier C, Haase KM, Brandl PA, Krumm SH (2017a). Primitive andesites from the Taupo Volcanic Zone formed by magma mixing. *Contributions to Mineralogy and Petrology* 172(5): 33. doi:10.1007/s00410-017-1354-0.

Beier C, Turner SP, Haase KM, Pearce JA, Münker C, Regelous M (2017b). Trace Element and Isotope Geochemistry of the Northern and Central Tongan Islands with an Emphasis on the Genesis of High Nb/Ta Signatures at the Northern Volcanoes of Tafahi and Niuatoputapu. *Journal of Petrology* 58(6): 1073–1106. doi:10.1093/petrology/egx047.

Beier C, Turner SP, Schoenhofen-Romer MV, Brandl PA, Haase KM, McGee L, Arculus RJ (2025). Geochemical glass data for the contribution: Identifying fluid-fluxed versus decompression melting in the Tonga island arc – Lau back arc region [dataset]. PANGAEA. doi:10.1594/PANGAEA.978496.

Beier C, Turner SP, Sinton JM, Gill JB (2010). Influence of subducted components on back-arc melting dynamics in the Manus Basin. *Geochemistry, Geophysics, Geosystems* 11: Q0AC03. doi:10.1029/2010gc003037.

Bevis M, Taylor FW, Schutz BE, Recy J, Isacks BL, Helu S, Singh R, Kendrick E, Stowell J, Taylor B, Calmantli S (1995). Geodetic observations of very rapid convergence and back-arc extension at the Tonga arc. *Nature* 374(6519): 249–251. doi:10.1038/374249a0.

Boespflug X, Dosso L, Bougault H, Joron JL (1990). Trace element and isotopic (Sr, Nd) Geochemistry of Volcanic Rocks from the Lau Basin. *Geologisches Jahrbuch Reihe D Mineralogie, Petrographie, Geochemie, Lagerstättenkunde* 92: 503–516.

Bourdon B, Turner S, Allegre C (1999). Melting dynamics beneath the Tonga-Kermadec island arc inferred from 231Pa- 235U systematics. *Science* 286(5449): 2491–2493. doi:10.1126/science.286.5449.2491.

Bourdon B, Turner S, Dosseto A (2003a). Dehydration and partial melting in subduction zones: Constraints from U-series disequilibria. *Journal of Geophysical Research: Solid Earth* 108(B6): n/a–n/a. doi:10.1029/2002JB001839.

Bourdon B, Turner SP, Henderson GM, Lundstrom CC (2003b). Introduction to U-series geochemistry. In *Uranium-series geochemistry*, vol. 52;, pp. 1–21. Mineralogical Society of America and Geochemical Society, Washington, DC, United States. doi:10.2113/0520001.

Brandl PA, Beier C, Regelous M, Abouchami W, Haase KM, Garbe-Schönberg D, Galer SJG (2012). Volcanism on the flanks of the East Pacific Rise: Quantitative constraints on mantle heterogeneity and melting processes. *Chemical Geology* 289-299(3-4): 41–56. doi:10.1016/j.chemgeo.2011.12.015.

Bézos A, Escrig S, Langmuir CH, Michael PJ, Asimow PD (2009). Origins of chemical diversity of back-arc basin basalts: A segment-scale study of the Eastern Lau Spreading Center. *Journal of Geophysical Research* 114(B06212). doi:10.1029/2008jb005924.

Cagnioncle AM, Parmentier EM, Elkins-Tanton LT (2007). Effect of solid flow above a subducting slab on water distribution and melting at convergent plate boundaries. *Journal of Geophysical Research: Solid Earth* 112(B9). doi:https://doi.org/10.1029/2007JB004934.

Castillo PR, Lonsdale PF, Moran CL, Hawkins JW (2009). Geochemistry of mid-Cretaceous Pacific crust being subducted along the Tonga-Kermadec Trench: Implications for the generation of arc lavas. *Lithos* 112(1-2): 87–102. doi:10.1016/j.lithos.2009.03.041.

Caulfield J, Turner S, Arculus R, Dale C, Jenner FE, Pearce J, Macpherson CG, Handley HK (2012). Mantle flow, volatiles, slab-surface temperatures and melting dynamics in the north Tonga arc–Lau back-arc basin. *Journal of Geophysical Research* 117(B11209). doi:10.1029/2012JB009526.

Chen JH, Lawrence Edwards R, Wasserburg GJ (1986). ^{238}U, ^{234}U and ^{232}Th in seawater. *Earth and Planetary Science Letters* 80(3-4): 241–251. doi:10.1016/0012-821X(86)90108-1.

Collier J, Sinha M (1990). Seismic images of a magma chamber beneath the Lau Basin back-arc spreading centre. *Nature* 346(6285): 646–648. doi:10.1038/346646a0.

Conder JA, Wiens DA, Morris J (2002). On the decompression melting structure at volcanic arcs and back-arc spreading centers. *Geophysical Research Letters* 29(15): 17–1 – 17 – 4. doi:10.1029/2002GL015390.

Cooper L, Plank T, Arculus R, Hauri E, Kelley KA (2022). Arc–Backarc Exchange Along the Tonga–Lau System: Constraints From Volatile Elements. *Journal of Petrology* 63(8): egac072. doi:10.1093/petrology/egac072.

Davies GF (1999). *Dynamic Earth; plates, plumes and mantle convection*. Cambridge University Press, Cambridge, United Kingdom. doi:10.1017/CBO9780511605802.

Davy B, Collot JY (2000). The Rapuhia Scarp (northern Hikurangi Plateau) - Its nature and subduction effects on the Kermadec Trench. *Tectonophysics* 328(3-4): 269–295. doi:10.1016/S0040-1951(00)00211-0.

Ding S, Plank T, Wallace PJ, Rasmussen DJ (2023). Sulfur_X: A Model of Sulfur Degassing During Magma Ascent. *Geochemistry, Geophysics, Geosystems* 24(4): e2022GC010552. doi:https://doi.org/10.1029/2022GC010552.

Dosseto A, Turner S, Douglas G (2006). Uranium-series isotopes in colloids and suspended sediments: Timescale for sediment production and transport in the Murray–Darling River system. *Earth and Planetary Science Letters* 246(3-4): 418–431. doi:10.1016/j.epsl.2006.04.019.

Dunn RA, Martinez F (2011). Contrasting crustal production and rapid mantle transitions beneath back-arc ridges. *Nature* 469(7329): 198–202. doi:10.1038/nature09690.

Elliott T (2004). Tracers of the Slab. *Inside the Subduction Factory* pp. 23–45. doi:10.1029/138GM03.

Escrig S, Bézos A, Goldstein S, Langmuir C, Michael P (2009). Mantle source variations beneath the Eastern Lau Spreading Center and the nature of subduction components in the Lau basin-Tonga arc system. *Geochemistry, Geophysics, Geosystems* 10(4): 1–33. doi:10.1029/2008GC002281.

Escrig S, Bézos A, Langmuir CH, Michael PJ, Arculus R (2012). Characterizing the effect of mantle source, subduction input and melting in the Fonualei Spreading Center, Lau Basin: Constraints on the origin of the boninitic signature of the back-arc lavas. *Geochemistry, Geophysics, Geosystems* 13(10): Q10008. doi:10.1029/2012GC004130.

Ewart A, Bryan WB, Chappell BW, Rudnick RL (1994). Regional geochemistry of the Lau-Tonga arc and backarc systems. In Hawkins JW, Parson LM, Allan JF, Abrahamsen N, Bednarz U, Blanc G, Bloomer SH, Boe R, Bruns TR, Bryan WB, Chaproniere GCH, Clift PD, Ewart A, Fowler MG, Hergt JM, Hodkinson RA, Lavoie DL, Ledbetter JK, MacLeod CJ, Nilsson K, Nishi H, Pratt CE, Quinterno PJ, Reynolds RR, Rothwell RG, Sager WW, Schoeps D, Soakai S, Styzen MJ, Maddox EM (eds.) *Proceedings of the Ocean Drilling Program, scientific results, Lau Basin; covering Leg 135 of the cruises of the drilling vessel JOIDES Resolution, Suva Harbor, Fiji, to Honolulu, Hawaii, sites 834-841, 17 December 1990-28 February 1991.*, vol. 135 of *Proceedings of the Ocean Drilling Program, Scientific Results*, pp. 385–425. Texas A & M University, Ocean Drilling Program, College Station, TX, United States. doi:10.2973/odp.proc.sr.135.141.1994.

Ewart A, Collerson KD, Regelous M, Wendt JI, Niu Y (1998). Geochemical evolution within the Tonga-Kermadec-Lau arc-back-arc systems; the role of varying mantle wedge composition in space and time. *Journal of Petrology* 39(3): 331–368. doi:10.1093/petrology/39.3.331.

Ewart A, Hawkesworth C (1987). The Pleistocene Recent Tonga Kermadec Arc Lavas - Interpretation of New Isotopic and Rare-Earth Data in Terms of a Depleted Mantle Source Model. *Journal of Petrology* 28(3): 495–530. doi:10.1093/petrology/28.3.495.

Falloon TJ, Malahoff A, Zonenshain LP, Bogdanov Y (1992). Petrology and Geochemistry of Back-Arc Basin Basalts from Lau Basin Spreading Ridges at 15°, 18° and 19° S. *Mineralogy and Petrology* 47(1): 1–35. doi:10.1007/Bf01165295.

Forsyth DW, Webb SC, Dorman LM, Shen Y (1998). Phase Velocities of Rayleigh Waves in the MELT Experiment on the East Pacific Rise. *Science* 280(5367): 1235–1238. doi:10.1126/science.280.5367.1235.

Frenzel G, Mühe R, Stoffers P (1990). Petrology of the volcanic rocks from the Lau Basin, Southwest Pacific; Petrologie der Vulkangesteine des Lau-Beckens, Südwest-Pazifik. ISBN: 0341-6429.

Fretzdorff S, Haase K (2002). Geochemistry and petrology of lavas from the submarine flanks of Réunion Island (western Indian Ocean): Implications for magma genesis and the mantle source. *Mineralogy and Petrology* 75(3-4): 153–184. doi:10.1007/s007100200022.

Fretzdorff S, Haase KM, Leat PT, Livermore RA, Garbe-Schönberg CD, Fietzke J, Stoffers P (2003). ^{230}Th- ^{238}U disequilibrium in East Scotia backarc basalts; implications for slab contributions. *Geology* 31(8): 693–696. doi:10.1130/G19469.1.

Fretzdorff S, Schwarz-Schampera U, Gibson HL, Garbe-Schönberg CD, Hauff F, Stoffers P (2006). Hydrothermal activity and magma genesis along a propagating back-arc basin: Valu Fa Ridge (southern Lau Basin). *Journal of Geophysical Research* 111(B8). doi:10.1029/2005JB003967.

Galley C, Baxter A, Hannington M, King M, Bethell E, Lelièvre P, Fassbender M, Jamieson J (2024). Quantifying Crustal Growth in Arc-Backarc Systems: Gravity Inversion Modeling of the Lau Basin. *Journal of Geophysical Research: Solid Earth* 129(12): e2024JB029013. doi:10.1029/2024JB029013.

George R, Turner S, Hawkesworth C, Morris J, Nye C, Ryan J, Zheng SH (2003). Melting processes and fluid and sediment transport rates along the Alaska-Aleutian arc from an integrated U-Th-Ra-Be isotope study. *Journal of Geophysical Research* 108(B5, 2252): doi:10.1029/2002JB001916. doi:10.1029/2002jb001916.

George R, Turner S, Morris J, Plank T, Hawkesworth CJ, Ryan J (2005). Pressure-temperature-time paths of sediment recycling beneath the Tonga-Kermadec arc. *Earth and Planetary Science Letters* 233(1-2): 195–211. doi:10.1016/j.epsl.2005.01.020.

Gill JB (1976). Composition and Age of Lau Basin and Ridge Volcanic-Rocks - Implications for Evolution of an Interarc Basin and Remnant Arc. *Geological Society of America Bulletin* 87(10): 1384–1395. doi:10.1130/0016-7606(1976)87<1384:Caaolb>2.0.Co;2.

Goldberg SL, Holt AF (2024). Characterizing the Complexity of Subduction Zone Flow With an Ensemble of Multiscale Global Convection Models. *Geochemistry, Geophysics, Geosystems* 25(2): e2023GC011134. doi:10.1029/2023GC011134.

Haase KA, Stroncik N, Garbe-Schönberg D, Stoffers P (2006). Formation of island are dacite magmas by extreme crystal fractionation: An example from Brothers Seamount, Kermadec island arc (SW Pacific). *Journal of Volcanology and Geothermal Research* 152(3-4): 316–330. doi:10.1016/j.jvolgeores.2005.10.010.

Haase KM, Fretzdorff S, Mühe R, Garbe-Schönberg D, Stoffers P (2009). A geochemical study of off-axis seamount lavas at the Valu Fa Ridge: Constraints on magma genesis and slab contributions in the southern Tonga subduction zone. *Lithos* 112(1-2): 137–148. doi:10.1016/j.lithos.2009.05.041.

Haase KM, Worthington TJ, Stoffers P, Garbe-Schönberg CD, Wright I (2002). Mantle dynamics, element recycling, and magma genesis beneath the Kermadec Arc-Havre Trough. *Geochemistry, Geophysics, Geosystems* 3(11): 1071. doi:10.1029/2002GC000335.

Hall PS, Kincaid C (2001). Diapiric flow at subduction zones: a recipe for rapid transport. *Science* 292(5526): 2472–2475. doi:10.1126/science.1060488.

Hawkins JW (1976). Petrology and Geochemistry of Basaltic Rocks of Lau Basin. *Earth and Planetary Science Letters* 28(3): 283–297. doi:10.1016/0012-821x(76)90190-4.

Hawkins JW (1995a). Evolution of the Lau Basin—Insights from ODP Leg 135. In *Active Margins and Marginal Basins of the Western Pacific*, Geophysical Monograph Series, pp. 125–173. American Geophysical Union. doi:10.1029/GM088p0125.

Hawkins JW (1995b). The Geology of the Lau Basin. In Taylor B (ed.) *Backarc Basins: Tectonics and Magmatism*, pp. 63–138. Springer US, Boston, MA. doi:10.1007/978-1-4615-1843-3_3.

Hawkins JW, Melchior JT (1985). Petrology of Mariana Trough and Lau Basin Basalts. *Journal of Geophysical Research-Solid Earth and Planets* 90(Nb13): 1431–1468. doi:10.1029/JB090iB13p11431.

Hayes GP, Wald DJ, Johnson RL (2012). Slab1. 0: A three-dimensional model of global subduction zone geometries. *Journal of Geophysical Research* 117(B1): B01302. doi:10.1029/2011JB008524.

Heinonen JS, Spera FJ, Bohrson WA (2021). Thermodynamic limits for assimilation of silicate crust in primitive magmas. *Geology* 50(1): 81–85. doi:10.1130/G49139.1.

Hergt JM, Hawkesworth CJ (1994). Pb-, Sr-, and Nd-isotopic evolution of the Lau Basin; implications for mantle dynamics during backarc opening. In Hawkins JW, Parson LM, Allan JF, Abrahamsen N, Bednarz U, Blanc G, Bloomer SH, Boe R, Bruns TR, Bryan WB, Chaproniere GCH, Clift PD, Ewart A, Fowler MG, Hergt JM, Hodkinson RA, Lavoie DL, Ledbetter JK, MacLeod CJ, Nilsson K, Nishi H, Pratt CE, Quinterno PJ, Reynolds RR, Rothwell RG, Sager WW, Schoeps D, Soakai S, Styzen MJ, Maddox EM (eds.) *Proceedings of the Ocean Drilling Program, scientific results, Lau Basin; covering Leg 135 of the cruises of the drilling vessel JOIDES Resolution, Suva Harbor, Fiji, to Honolulu, Hawaii, sites 834-841, 17 December 1990-28 February 1991.*, vol. 135 of *Proceedings of the Ocean Drilling Program, Scientific Results*, pp. 505–517. Texas A & M University, Ocean Drilling Program, College Station, TX, United States.

Hergt JM, Woodhead JD (2007). A critical evaluation of recent models for Lau-Tonga arc-backarc basin magmatic evolution. *Chemical Geology* 245(1-2): 9–44. doi:10.1016/j.chemgeo.2007.07.022.

Hilton DR, Hammerschmidt K, Loock G, Friedrichsen H (1993). Helium and argon isotope systematics of the central Lau Basin and Valu Fa Ridge: Evidence of crust/mantle interactions in a back-arc basin. *Geochimica et Cosmochimica Acta* 57(12): 2819–2841. doi:10.1016/0016-7037(93)90392-A.

Hirth G, Kohlstedt DL (1996). Water in the oceanic upper mantle; implications for rheology, melt extraction and the evolution of the lithosphere. *Earth and Planetary Science Letters* 144(1-2): 93–108. doi:10.1016/0012-821x(96)00154-9.

Jacobs AM, Harding AJ, Kent GM (2007). Axial crustal structure of the Lau back-arc basin from velocity modeling of multichannel seismic data. *Earth and Planetary Science Letters* 259(3-4): 239–255.

Jenner F, O'Neill H (2012). Analysis of 60 elements in 616 ocean floor basaltic glasses. *Geochemistry Geophysics Geosystems* 13: Q02005. doi:10.1029/2011GC004009.

Jenner GA, Cawood PA, Rautenschlein M, White WM (1987). Composition of Back-Arc Basin Volcanics, Valu Fa Ridge, Lau Basin - Evidence for a Slab-Derived Component in Their Mantle Source. *Journal of Volcanology and Geothermal Research* 32(1-3): 209–222. doi:10.1016/0377-0273(87)90045-X.

Johnson MC, Plank T (2000). Dehydration and melting experiments constrain the fate of subducted sediments. *Geochemistry, Geophysics, Geosystems* 1(12): 1007. doi:10.1029/1999GC000014.

Jull M, Kelemen PB, Sims K (2002). Consequences of diffuse and channelled porous melt migration on uranium series disequilibria. *Geochimica et Cosmochimica Acta* 66(23): 4133–4148. doi:10.1016/S0016-7037(02)00984-5.

Karrei LI (2008). *Elevated Pt, Pd and Au concentrations in High-Ca Boninites from the Northern Tonga Arc: evidence for retention of monosulfide solid solution in the source, and the involvement of four independent components during petrogenesis*. Phd thesis, University of Toronto, Toronto, Canada.

van Keken PE, Hacker BR, Syracuse EM, Abers GA (2011). Subduction factory: 4. Depth-dependent flux of H_2O from subducting slabs worldwide. *Journal of Geophysical Research-Solid Earth* 116(B1). doi:10.1029/2010jb007922.

Keller N, Arculus R, Hermann J, Richards S (2008). Submarine back-arc lava with arc signature: Fonualei Spreading Center, northeast Lau Basin, Tonga. *Journal of Geophysical Research* 113(B8): 28. doi:10.1029/2007JB005451.

Kelley KA, Plank T, Newman S, Stolper EM, Grove TL, Parman S, Hauri EH (2010). Mantle Melting as a Function of Water Content beneath the Mariana Arc. *Journal of Petrology* 51(8): 1711–1738. doi:10.1093/petrology/egq036.

Kent AJ, Peate DW, Newman S, Stolper EM, Pearce JA (2002). Chlorine in submarine glasses from the Lau Basin: seawater contamination and constraints on the composition of slab-derived fluid. *Earth and Planetary Science Letters* 202(2): 361–377. doi:10.1016/S0012-821x(02)00786-0.

Kessel R, Schmidt MW, Ulmer P, Pettke T (2005). Trace element signature of subduction-zone fluids, melts and supercritical liquids at 120-180 km depth. *Nature* 437(7059): 724–727. doi:10.1038/nature03971.

Kimura JI (2017). Modeling chemical geodynamics of subduction zones using the Arc Basalt Simulator version 5. *Geosphere* 13(4): 992–1025. doi:10.1130/Ges01468.1.

Kimura JI, Ariskin AA (2014). Calculation of water-bearing primary basalt and estimation of source mantle conditions beneath arcs: PRIMACALC2 model for WINDOWS. *Geochemistry, Geophysics, Geosystems* 15(4): 1494–1514. doi:10.1002/2014GC005329.

Langmuir CH, Bézos A, Escrig S, Parman S (2006). Chemical systematics and hydrous melting of the mantle in back-arc basins. In Christie DM, Fisher CR, Lee SM, Givens S (eds.) *Geophysical Monograph Series*, vol. 166, pp. 87–146. American Geophysical Union, Washington DC. doi:10.1029/166GM07.

Le Maitre R (1989). *A classification of igneous rocks and glossary of terms, recommendations of the International union of geological sciences, subcomission on the systematics of igneous rocks.* Blackwell, Oxford, London.

Ligi M, Cuffaro M, Chierici F, Calafato A (2008). Three-dimensional passive mantle flow beneath mid-ocean ridges: An analytical approach. *Geophysical Journal International* 175(2): 783–805. doi:10.1111/j.1365-246X.2008.03931.x.

Loock G, Mcdonough WF, Goldstein SL, Hofmann AW (1990). Isotopic Compositions of Volcanic Glasses from the Lau Basin. *Marine Mining* 9(2): 235–245.

Lundstrom CC (2003). Uranium-series Disequilibria in Mid-ocean Ridge Basalts: Observations and Models of Basalt Genesis. In Bourdon B, Henderson GM, Lundstrom C, Turner SP (eds.) *Uranium-series geochemistry*, vol. 52 of *Reviews in Mineralogy and Geochemistry*, pp. 175–214. Mineralogical Society of America, Washington. doi:10.1515/9781501509308-010.

Marschall HR, Schumacher JC (2012). Arc magmas sourced from mélange diapirs in subduction zones. *Nature Geoscience* 5(11): 1–6. doi:10.1038/ngeo1634.

Massoth G, Baker E, Worthington T, Lupton J, de Ronde C, Arculus R, Walker S, Nakamura K, Ishibashi J, Stoffers P, Resing J, Greene R, Lebon G (2007). Multiple hydrothermal sources along the south Tonga arc and Valu Fa Ridge. *Geochemistry Geophysics Geosystems* 8. doi:10.1029/2007gc001675.

McDonough W, Sun SS (1995). The composition of the Earth. *Chemical Geology* 120(3-4): 223–253. doi:10.1016/0009-2541(94)00140-4.

McGee L, Beier C, Smith I, Turner S (2011). Dynamics of melting beneath a small-scale basaltic system: a U–Th–Ra study from Rangitoto volcano, Auckland volcanic field, New Zealand. *Contributions to Mineralogy and Petrology* 162(3): 547–563. doi:10.1007/s00410-011-0611-x.

Morton J, Pohl W (1990). Magnetic anomaly identification in the Lau basin and North Fiji basin, southwest Pacific ocean. *Geologisches Jahrbuch Reihe D Mineralogie, Petrographie, Geochemie, Lagerstättenkunde* 92: 93–108.

Morton JL, Sleep NH (1985). Seismic reflections from a Lau Basin magma chamber. In Scholl D, Vallier T (eds.) *Geology and offshore resources of Pacific island arcs–Tonga region*, vol. 2 of *Mineral Resources Earth Science Series*, pp. 441–453. Circum-Pacific Council for Energy and Mineral Resources, Houston, Texas.

Newman S, Lowenstern JB (2002). VolatileCalc: a silicate melt–H_2O–CO_2 solution model written in Visual Basic for excel. *Computers & Geosciences* 28(5): 597–604. doi:10.1016/s0098-3004(01)00081-4.

Pearce JA, Ernewein M, Bloomer SH, Parson LM, Murton BJ, Johnson LE (1994). Geochemistry of Lau Basin volcanic rocks: influence of ridge segmentation and arc proximity. *Geological Society, London, Special Publications* 81(1): 53–75. doi:10.1144/gsl.sp.1994.081.01.04.

Pearce JA, Parkinson IJ (1993). Trace element models for mantle melting: application to volcanic arc petrogenesis. *Geological Society, London, Special Publications* 76(1): 373–403. doi:10.1144/GSL.SP.1993.076.01.19.

Pearce JA, Peate DW (1995). Tectonic Implications of the Composition of Volcanic Arc Magmas. *Annual Review of Earth and Planetary Sciences* 23(1): 251–285. doi:10.1146/annurev.ea.23.050195.001343.

Pearce JA, Stern RJ (2006). Origin of back-arc basin magmas: Trace element and isotope perspectives. In Christie DM (ed.) *Back-Arc Spreading Systems: Geological, Biological, Chemical, and Physical Interactions*, vol. 166, pp. 63–86. Washington D.C. doi:10.1029/166gm06.

Pearce JA, Stern RJ, Bloomer SH, Fryer P (2005). Geochemical mapping of the Mariana arc-basin system: Implications for the nature and distribution of subduction components. *Geochemistry Geophysics Geosystems* 6(7). doi:10.1029/2004GC000895.

Peate DW, Kokfelt TF, Hawkesworth CJ, Van Calsteren PW, Hergt JM, Pearce JA (2001). U-series isotope data on Lau Basin glasses: the role of subduction-related fluids during melt generation in back-arc basins. *Journal of Petrology* 42(8): 1449–1470. doi:10.1093/petrology/42.8.1449.

Plank T, Langmuir CH (1993). Tracing trace elements from sediment input to volcanic output at subduction zones. *Nature* 362: 739–743. doi:10.1038/362739a0.

Plank T, Langmuir CH (1998). The chemical composition of subducting sediment and its consequences for the crust and mantle. *Chemical Geology* 145(3-4): 325–394. doi:10.1016/S0009-2541(97)00150-2.

Portnyagin M, Hoernle K, Plechov P, Mironov N, Khubunaya S (2007). Constraints on mantle melting and composition and nature of slab components in volcanic arcs from volatiles (H_2O, S, Cl, F) and trace elements in melt inclusions from the Kamchatka Arc. *Earth and Planetary Science Letters* 255(1): 53–69. doi:10.1016/j.epsl.2006.12.005.

Regelous M, Collerson KD, Ewart A, Wendt JI (1997). Trace element transport rates in subduction zones; evidence from Th, Sr and Pb isotope data for Tonga-Kermadec Arc lavas. *Earth and Planetary Science Letters* 150(3-4): 291–302. doi:10.1016/S0012-821x(97)00107-6.

Schmid F, Kopp H, Schnabel M, Dannowski A, Heyde I, Riedel M, Hannington MD, Engels M, Beniest A, Klaucke I, Augustin N, Brandl PA, Devey C (2020). Crustal Structure of the Niuafo'ou Microplate and Fonualei Rift and Spreading Center in the Northeastern Lau Basin, Southwestern Pacific. *Journal* *of Geophysical Research: Solid Earth* 125(6): e2019JB019184. doi:10.1029/2019JB019184.

Scott SR, Sims KWW, Reagan MK, Ball L, Schwieters JB, Bouman C, Lloyd NS, Waters CL, Standish JJ, Tollstrup DL (2019). The application of abundance sensitivity filters to the precise and accurate measurement of uranium series nuclides by plasma mass spectrometry. *International Journal of Mass Spectrometry* 435: 321–332. doi:10.1016/j.ijms.2018.11.011.

Sims KWW, Pichat S, Reagan MK, Kyle PR, Dulaiova H, Dunbar NW, Prytulak J, Sawyer G, Layne GD, Blichert-Toft J, Gauthier PJ, Charette MA, Elliott TR (2013). On the Time Scales of Magma Genesis, Melt Evolution, Crystal Growth Rates and Magma Degassing in the Erebus Volcano Magmatic System Using the ^{238}U, ^{235}U and ^{232}Th Decay Series. *Journal of Petrology* 54(2): 235–271. doi:10.1093/petrology/egs068.

Sleeper JD, Martinez F (2014). Controls on segmentation and morphology along the back-arc Eastern Lau Spreading Center and Valu Fa Ridge. *Journal of Geophysical Research: Solid Earth* 119(3): 1678–1700. doi:10.1002/2013JB010545.

Sleeper JD, Martinez F, Arculus R (2016). The Fonualei Rift and Spreading Center: Effects of ultraslow spreading and arc proximity on back-arc crustal accretion. *Journal of Geophysical Research: Solid Earth* 121(7): 4814–4835. doi:10.1002/2016JB013050.

Spandler C, Mavrogenes J, Hermann J (2007). Experimental constraints on element mobility from subducted sediments using high-P synthetic fluid/melt inclusions. *Chemical Geology* 239(3–4): 228–249. doi:10.1016/j.chemgeo.2006.10.005.

Spandler C, Pirard C (2013). Element recycling from subducting slabs to arc crust: A review. *Lithos* 170–171: 208–223. doi:10.1016/j.lithos.2013.02.016.

von Stackelberg U, Marchig V, Müller P, Weiser T (1990). Hydrothermal mineralization in the Lau and North Fiji basins. *Geologisches Jahrbuch Reihe D Mineralogie, Petrographie, Geochemie, Lagerstättenkunde* 92: 547–613.

Stewart MS, Hannington MD, Emberley J, Baxter AT, Krätschell A, Petersen S, Brandl PA, Anderson MO, Mercier-Langevin P, Mensing R, Breker K, Fassbender ML (2022). A new geological map of the Lau Basin (southwestern Pacific Ocean) reveals crustal growth processes in arc-backarc systems. *Geosphere* 18(2): 910–943. doi:10.1130/GES02340.1.

Stoffers P, Worthington TJ, Schwarz-Schampera U, Ackermand D, Beaudoin Y, Bigalke N, Fretzdorff S, Gibson HL, Hekinian R, Kindermann A, Kuhn T, Main W, Schreiber K, Timm C, Tonga'onevai S, Türkay M, Unverricht D, Vailea A, Zimmerer M (2003). Cruise Report SONNE 167 Louisville Ridge: Dynamics and Magmatism of a mantle plume and its influence on the Tonga-Kermadec subduction system. *Report*, Institut für Geowissenschaften, Universität Kiel.

Sykes LR (1966). The seismicity and deep structure of Island arcs. *Journal of Geophysical Research (1896-1977)* 71(12): 2981–3006. doi:10.1029/JZ071i012p02981.

Syracuse EM, van Keken PE, Abers GA (2010). The global range of subduction zone thermal models. *Physics of the Earth and Planetary Interiors* 183(1–2): 73–90. doi:10.1016/j.pepi.2010.02.004.

Tatsumi Y, Eggins S (1995). Subduction Zone Magmatism. In *Subduction zone magmatism*. Blackwell Science; Frontiers in Earth Sciences.

Taylor B, Martinez F (2003). Back-arc basin basalt systematics. *Earth and Planetary Science Letters* 210(3-4): 481–497. doi:10.1016/S0012-821X(03)00167-5.

Taylor B, Zellmer K, Martinez F, Goodliffe A (1996). Sea-floor spreading in the Lau back-arc basin. *Earth and Planetary Science Letters* 144(1): 35–40. doi:10.1016/0012-821X(96)00148-3.

The MELT Seismic Team (1998). Imaging the Deep Seismic Structure Beneath a Mid-Ocean Ridge: The MELT Experiment. *Science* 280(5367): 1215–1218. doi:10.1126/science.280.5367.1215.

The Nautilau Group (1990). Hydrothermal activity in the Lau Basin: First results from the NAUTILAU Cruise. *Eos, Transactions American Geophysical Union* 71(18): 678–679. doi:10.1029/90EO00166.

Tian L, Castillo PR, Hawkins JW, Hilton DR, Hanan BB, Pietruszka AJ (2008). Major and trace element and Sr-Nd isotope signatures of lavas from the Central Lau Basin: Implications for the nature and influence of subduction components in the back-arc mantle. *Journal of Volcanology and Geothermal Research* 178(4): 657–670. doi:10.1016/j.jvolgeores.2008.06.039.

Timm C, Leybourne MI, Hoernle K, Wysoczanski RJ, Hauff F, Handler M, Tontini FC, de Ronde CEJ (2016). Trench-perpendicular Geochemical Variation Between two Adjacent Kermadec Arc Volcanoes Rumble II East and West: the Role of the Subducted Hikurangi Plateau in Element Recycling in Arc Magmas. *Journal of Petrology* 57(7): 1335–1360. doi:10.1093/petrology/egw042.

Tollstrup D, Gill J, Kent A, Prinkey D, Williams R, Tamura Y, Ishizuka O (2010). Across-arc geochemical trends in the Izu-Bonin arc: Contributions from the subducting slab, revisited. *Geochemistry Geophysics Geosystems* 11(1): Q01X10–. doi:10.1029/2009GC002847.

Turner M, Ireland T, Hermann J, Holden P, Padrón-Navarta JA, Hauri EH, Turner S (2015). Sensitive high resolution ion microprobe – stable isotope (SHRIMP-SI) analysis of water in silicate glasses and nominally anhydrous reference minerals. *Journal of Analytical Atomic Spectrometry* 30(8): 1706–1722. doi:10.1039/C5JA00047E.

Turner S, Beier C, Niu Y, Cook C (2011). U-Th-Ra disequilibria and the extent of off-axis volcanism across the East Pacific Rise at 9°30'N, 10°30'N, and 11°20'N. *Geochemistry, Geophysics, Geosystems* 12(7): Q0AC12. doi:10.1029/2010gc003403.

Turner S, Bourdon B, Gill JB (2003). Insights into magma genesis at convergent margins from U-series isotopes. In Bourdon B, Henderson GM, Lundstrom C, Turner SP (eds.) *Uranium-series geochemistry*, vol. 52 of *Reviews in Mineralogy and Geochemistry*, pp. 255–310. Mineralogical Society of America, Washington. doi:10.2113/0520255.

Turner S, Evans P, Hawkesworth CJ (2001). Ultrafast source-to-surface movement of melt at island arcs from ^{226}Ra-^{230}Th systematics. *Science* 292(5520): 1363–1366. doi:10.1126/science.1059904.

Turner S, Hawkesworth C (1997). Constraints on flux rates and mantle dynamics beneath island arcs from Tonga-Kermadec lava geochemistry. *Nature* 389(6651): 568–573. doi:10.1038/39257.

Turner S, Regelous M, Black S, George R, Hawkesworth C (2004). U-Series Isotope Constraints on Melting Processes and Degassing Time Scales at Island Arc Volcanoes. In *17th Australian Geological Convention*, p. 295. Sydney, N.S.W., Australia.

Turner S, Regelous M, Hawkesworth C, Rostami K (2006). Partial melting processes above subducting plates: Constraints from ^{231}Pa–^{235}U disequilibria. *Geochimica et Cosmochimica Acta* 70(2): 480–503. doi:10.1016/j.gca.2005.09.004.

Vallier TL, Jenner GA, Frey FA, Gill JB, Davis AS, Volpe AM, Hawkins JW, Morris JD, Cawood PA, Morton JL, Scholl DW, Rautenschlein M, White WM, Williams RW, Stevenson AJ, White LD (1991). Subalkaline andesite from Valu Fa Ridge, a back-arc spreading center in southern Lau Basin; petrogenesis, comparative chemistry, and tectonic implications. *Chemical Geology* 91(3): 227–256. doi:10.1016/0009-2541(91)90002-9.

Wei SS, Wiens DA, van Keken PE, Cai C (2017). Slab temperature controls on the Tonga double seismic zone and slab mantle dehydration. *Science Advances* 3(1): e1601755. doi:10.1126/sciadv.1601755.

Wei SS, Wiens DA, Zha Y, Plank T, Webb SC, Blackman DK, Dunn RA, Conder JA (2015). Seismic evidence of effects of water on melt transport in the Lau back-arc mantle. *Nature* 518(7539): 395–8. doi:10.1038/nature14113.

Wiedicke M, Collier J (1993). Morphology of the Valu Fa Spreading Ridge in the Southern Lau Basin. *Journal of Geophysical Research-Solid Earth* 98(B7): 11769–11782. doi:10.1029/93jb00708.

Woodhead JD, Eggins SM, Johnson RW (1998). Magma genesis in the New Britain island arc: Further insights into melting and mass transfer processes. *Journal of Petrology* 39(9): 1641–1668. doi:10.1093/petrology/39.9.1641.

Workman RK, Hart SR (2005). Major and trace element composition of the depleted MORB mantle (DMM). *Earth and Planetary Science Letters* 231(1-2): 53–72. doi:10.1016/j.epsl.2004.12.005.

Wu F, Turner S, Schaefer BF (2020). Mélange versus fluid and melt enrichment of subarc mantle: A novel test using barium isotopes in the Tonga-Kermadec arc. *Geology* 48(11): 1053–1057. doi:10.1130/G47549.1.

Zellmer K, Taylor B (2001). A three-plate kinematic model for Lau Basin opening. *Geochemistry Geophysics Geosystems* 2: 2000GC000106. doi:10.1029/2000GC000106.

Zha Y, Webb SC, Wei SS, Wiens DA, Blackman DK, Menke W, Dunn RA, Conder JA (2014). Seismological imaging of ridge–arc interaction beneath the Eastern Lau Spreading Center from OBS ambient noise tomography. *Earth and Planetary Science Letters* 408(0): 194–206. doi:10.1016/j.epsl.2014.10.019.

Zhang N, Behn MD, Parmentier EM, Kincaid C (2020). Melt Segregation and Depletion During Ascent of Buoyant Diapirs in Subduction Zones. *Journal of Geophysical Research: Solid Earth* 125(2): e2019JB018203. doi:10.1029/2019JB018203.

Zhao D, Xu Y, Wiens DA, Dorman LM, Hildebrand J, Webb SC (1997). Depth extent of the Lau back-arc spreading center and its relation to subduction processes. *Science* 278(5336): 254–257. doi:10.1126/science.278.5336.254.